

Title: Chronic embedded cortico-thalamic closed-loop deep brain stimulation for the treatment of essential tremor

Authors: Enrico Opri^{1*}, Stephanie Cernera¹, Rene Molina², Robert Eisinger³, Jackson Cagle¹, Leonardo Almeida³, Timothy Denison⁴, Michael S. Okun³, Kelly D. Foote^{3Ψ}, Aysegul Gunduz^{1,2,3Ψ}

Affiliations:

¹ J. Ccrayton Pruitt Family Department of Biomedical Engineering, University of Florida, Gainesville, FL 32611, USA

² Electrical and Computer Engineering, University of Florida, Gainesville, FL 32603, USA

³ Norman Fixel Institute for Neurological Diseases at UF Health, Departments of Neurology and Neurosurgery, University of Florida, Gainesville, FL 32608, USA

⁴ Department of Engineering Science, University of Oxford, Oxford OX1 3PJ, United Kingdom

Ψ This paper was a product of the NIH BRAIN Initiative and the Multi-PI's Foote and Gunduz serve as co-senior authors.

*Correspondence to: enrico.opri@ufl.edu.

One Sentence Summary: Effective tremor suppression in ET with half the energy requirements was achieved by on-demand DBS based on real-time cortical sensing.

Abstract: Deep brain stimulation (DBS) is an approved therapy for the treatment of medically-refractory and severe movement disorders. However, most existing neurostimulators can only apply continuous stimulation (open-loop DBS, OL-DBS), ignoring patient behavior and environmental factors, which consequently leads to an inefficient therapy, thus limiting the therapeutic window. Here, we established the feasibility of a self-adjusting therapeutic DBS (closed-loop DBS, CL-DBS), fully embedded in a chronic investigational neurostimulator (Activa PC+S), for 3 patients affected by essential tremor (ET) enrolled in a longitudinal (6 months) within-subject crossover protocol (DBS OFF, OL-DBS, CL-DBS). Most patients with ET experience involuntary limb tremor during goal-directed movements, but not during rest. Hence, the proposed CL-DBS paradigm explored the efficacy of modulating the stimulation-amplitude based on patient-specific motor behavior, suppressing the pathological tremor on-demand based on a cortical electrode detecting upper-limb motor activity. Herein, we demonstrated how the proposed stimulation paradigm was able to achieve clinical efficacy and tremor suppression comparable with OL-DBS in a range of movements (cup reaching, proximal and distal posture, water pouring, writing), while having a consistent reduction in energy delivery. The proposed paradigm is an important step towards a behaviorally modulated fully embedded DBS system, capable of delivering stimulation only when needed, and potentially mitigating pitfalls of OL-DBS, such as DBS-induced side effects and premature device replacement.

[Main Text:]

Introduction

Current commercially available deep brain stimulation (DBS) devices effectively suppress debilitating tremor in movement disorders such as essential tremor (ET) and Parkinson's disease. Yet, current stimulation approaches (continuous stimulation, also known as open-loop stimulation) lack integration with patient behavior and environmental factors. Such lack of flexibility leads to unnecessary, constant stimulation and is likely associated with a higher incidence of DBS-related side effects, such as impaired proprioception, gait issues, or speech dysfunction (1–5). In addition, current literature has revealed that current open-loop paradigms may contribute to stimulation tolerance (6, 7). In the absence of tremor, ongoing continuous DBS delivery translates to a wasteful energy management and consequently to an excessive incidence of battery replacement surgeries. Furthermore, current standard of care requires labor-intensive adjustment of stimulation parameters in order to achieve the desired magnitude of tremor reduction while minimizing side effects. If this result cannot be achieved with one parameter setting, a patient may have to actively switch between a configuration optimized for maximal tremor suppression, and a less aggressive one with modest tremor suppression but with fewer side effects. For example, patients may choose the first configuration for writing or eating as it results in minimal tremor, and switch to the latter when speaking to reduce the stimulation-induced speech dysfunction. Thus, there is a critical need for advances in DBS technology with a focus on decoupling both the patient and clinician from continuous adjustments. Therefore, our work aims to deliver a “set and forget” approach to DBS, which independently self-adjusts based on real-time tracking of motor behavior.

In this study, we focused on ET, which is among the most common movement disorders and the most prevalent tremor disorder (8). ET is a progressive, degenerative brain disorder that results in increasingly debilitating tremor, and afflicts an estimated 7 million people in the US (2.2% of the population) (9) and from 0.4% to 6.3% of people worldwide (10). ET is directly linked to progressive functional impairment (11, 12), social embarrassment (12, 13), and even depression (14). ET is defined as a bilateral, rhythmical, involuntary oscillatory (~4-12 Hz) movement of the upper limbs (15). The subjects in our study were disabled by the intention tremor subtype of ET, which typically occurs in the hands and arms during the initiation and execution of goal-directed reaching motions, while it is absent or non-disabling at rest (16, 17). In spite of the numerous therapeutic modalities available (18), the effectiveness of non-surgical treatment options (medications, botox, assistive devices) in moderate to severe tremor has been disappointing (19–21). Additionally, 65% of those suffering from upper limb tremor report serious difficulties during their daily lives (22). For medically refractory and severe tremor patients, DBS has been widely adopted as a treatment option. A pathological synchronous oscillation in a neuronal network involving mainly the ventralis intermediate nucleus (VIM) of the thalamus, the premotor (PM), the primary motor (M1) cortices, and the cerebellum has been suggested (23, 24). Hence, the most common target for ET DBS therapy is the VIM thalamus (25).

This work introduces a chronically implanted and fully embedded closed-loop DBS paradigm for patients affected by ET, tailoring the device to suppress the pathological phenotype of interest (tremor) only when present. We used Activa PC+S bidirectional neurostimulators (Medtronic) that allow chronic recordings (26, 27) and prototyping of closed-loop therapies. We focused on detecting movement onset/termination for stimulation delivery on-demand. This was possible as

the tremor always manifested with movement. We considered that movement onset preceded tremor presentation and we therefore planned to deliver stimulation as rapidly as possible using detection of movement onset/termination through a subdural electrode array placed over the hand motor area. Together with a bidirectional neurostimulator connected to a standard DBS electrode array in the VIM, it enabled cortically-driven on-demand thalamic stimulation.

Results

Device implantation and offline feasibility.

To evaluate the feasibility of closed-loop in patients affected by ET, we implanted the Activa PC+S neurostimulators in 3 subjects affected by ET (Table S1), and evaluated the embedded control algorithm performances longitudinally (6 months). We designed an algorithm to drive stimulation with detection of movement execution, using low frequency oscillations (LFO) recorded from unilateral subdural cortical electrodes. The cortical target was the M1 hand motor region ipsilateral to the VIM lead, both contralateral to the most affected hand. Details of the cortical electrode positioning are shown in Figure 1A-C, respectively for subjects ET01, ET02, and ET03. Thalamic DBS leads positioning are shown in Figure 1D normalized to an MNI brain, together with structures of interest. The system was implemented by first training the algorithm parameters offline with data streamed using a telemetry wand (Nexus-D) (28) (setup described in Fig. 2A), collected during a cued arm movement task (both left and right arm) (task timeline shown in Fig. 2B, single data collection and related training shown in Fig. 2C, 2D). Next, it was tested online with the embedded classifier within Activa PC+S (26, 27). This prototyping strategy is described in Supplementary Material and Methods and in previous work (28, 29). In addition to user-driven algorithm requirements, we also implemented risk mitigations for the closed-loop design to limit the impact of potential hazards (Material and Methods: Risk and Mitigations, (30)). The subjects were left on the continuous conventional DBS (OL-DBS) settings between monthly visits during this feasibility study. Each month, for 6 months, OL-DBS settings were compared to closed-loop DBS settings in-clinic. The closed-loop settings were chosen with equal or decreased parameters (such as decreasing amplitude, stimulation frequency, and pulse width) to avoid any off-target stimulation side effects, such as paresthesia during stimulation onset. The preferred parameter reduction involved the pulse width, which has the benefit of reducing current spread and reducing stimulation induced paresthesia (31, 32). Patient tolerance to closed-loop stimulation was chosen as a hard constraint (go/no go milestone) considering that for closed-loop stimulation to be a viable therapeutic option, patient comfort had to be as important as tremor suppression. The data collected postoperatively demonstrated the possibility of achieving single-trial detection of movement execution, during cued (task timeline in Fig. 3A) and volitional movement trials, using contacts over M1 and VIM (Fig. 3B, 3C, 3D). Similarly to previous work involving patients affected by ET (33), there was a clear power deviation during movement in the cortical M1 activity (decrease in LFO, increase in high broadband activity above 60 Hz) (Fig. 3B top spectrogram, 3C left). The power deviation during movement in the VIM activity (decrease in LFO) (Fig. 3B bottom spectrogram, 3C right) could have been sufficient to achieve movement detection without relying on the cortical M1 activity; however, it was not a viable option as the stimulation overwhelmed the amplifier stage for the VIM channel, leading to unrecoverable brain activity from contacts adjacent to the stimulating contact within the same DBS lead (saturated VIM channel shown in Fig. S1). However, even during stimulation it was possible to recover viable spectral changes from the cortical contacts during a cued movement task (Fig. S2). To be able to minimize stimulation artifacts, the closed-

loop implementation was based only on the M1 contacts and a VIM bipolar stimulation paradigm, as monopolar stimulation resulted in excessive contamination of M1 power estimates.

Longitudinal clinical efficacy of closed-loop DBS compared with open-loop

Clinical outcomes were evaluated at each monthly visit for six months, for each of the DBS settings: DBS OFF, OL-DBS, and closed-loop DBS (CL-DBS). The settings used during each month are reported in Table S2. Clinical efficacy was determined using the Fahn-Tolosa-Marin Tremor Rating Scale (TRS) (34, 35), where the best outcome was associated with the lowest score. For the evaluation of the effectiveness of the DBS programming, only Part A (assesses examiner reported tremor location/severity) and Part B (assesses examiner-reported functional disability related to tremor) were taken into consideration. Part A and B of the TRS assessment include testing for water pouring, writing, spiral and line drawing, finger-to-nose, proximal and distal posture of the upper limbs, standing, and face/neck tremor. Video recordings were collected during the administration of the TRS and rated by a blinded neurologist. The operators configuring the stimulation could not be blinded because of the complexity of the setup; however, they were not involved in clinical scoring. The patient may have not been completely blinded regarding the DBS setting in use based on the incidence of paresthesia. Few OL-DBS settings, such as monopolar stimulation which was a common setting in the initial months (Table S2), caused temporary paresthesia when activated, resolving under 1 minute. The optimized CL-DBS settings used during TRS evaluation did not cause paresthesia, and consequently were not distinguishable from the DBS OFF settings and the late OL-DBS settings. The overall scores for the total body TRS revealed (Fig. 4A) a clear score decrease (improvement) of OL-DBS (mixed model ANOVA with patient as random effect, total TRS $F_{1,31}=38.182$, $P=7.377\text{e-}07$, contralateral side TRS $F_{1,31}=32.476$, $P=2.898\text{e-}06$) and CL-DBS (mixed model ANOVA with patient as random effect, total TRS $F_{1,24}=20.645$, $P=0.00013$, contralateral side TRS $F_{1,24}=18.529$, $P=0.00024$) compared to DBS OFF for all 3 patients. The percent decrease from DBS OFF was -33.8% (SD=17.8%) for total TRS (for contralateral side TRS was -52.7% [SD=26.9%]) with OL-DBS, whereas with CL-DBS was -32.7% (SD=12.7%) for total TRS (for contralateral side TRS there was a -47.4% [SD=14.3%] decrease). OL-DBS TRS score did not show statistical difference from CL-DBS (total TRS $t_7=0.000$, $p=1.000$, contralateral only TRS $t_7=-0.6070$, $p=0.5630$). A two one-sided t-test (TOST) procedure showed equivalence in clinical efficacy for OL-DBS and CL-DBS within a 2 TRS point interval (total TRS lower equivalence bound $t_7=4.7329$ $P=0.0011$, upper equivalence bound $t_7=-4.7329$ $P=0.0011$; contralateral side TRS lower equivalence bound $t_7=4.2488$, $P=0.0019$, upper equivalence bound $t_7=-5.4628$, $P=0.0005$). The 2 TRS point interval was chosen considering 1 point of uncertainty for each TRS test in the comparison (1 for OL-DBS and 1 for CL-DBS), which corresponds to 1.72% of the maximum score possible (116 points for the total TRS and 5% of the maximum score possible 40 for the contralateral side TRS).

Sensor-based tremor quantification during closed-loop DBS compared with open-loop

Additionally, we report tremor amplitude changes during both therapies using accelerometry data (Fig. 4B), as described in previous work (36, 37). Consistent with TRS scores (Fig. 4A), the accelerometry of the affected limb (limb contralateral to the DBS lead) showed a clear decrease (improvement) of OL-DBS (mixed model ANOVA with patient as random effect, $F_{1,29}=8.9479$, $P=0.0056$) and CL-DBS (mixed model ANOVA with patient as random effect, $F_{1,23}=6.1502$, $P=0.0209$) compared to DBS OFF for all 3 patients. The tremor amplitude percent decrease from DBS OFF was -42.8 (SD=23.6) % with OL-DBS, whereas with CL-DBS was -44.4 (SD=16.3)

% OL-DBS tremor amplitude did not show statistical difference from CL-DBS tremor amplitude ($t_7=1.1276$, $p=0.297$). TOST procedure showed equivalence in tremor amplitude for OL-DBS - CL-DBS within a 0.1 m/s^2 point interval (lower equivalence bound $t_7=4.1061$, $P=0.0023$, upper equivalence bound $t_7=-2.3433$, $P=0.0258$). The 0.1 points TRS interval was chosen considering estimation uncertainty and the minimum sensible difference for tremor severity considerations (37). We further segmented the movement and stimulation delivery in subintervals marked by event of interest, such as the stimulation onset (SO), the time when the stimulation reached its maximum amplitude (maximum stimulation amplitude reached, MSAR), and the movement onset (MO) (described in Fig. 4C). We then focused our interest on the tremor amplitude from MO to MSAR (interval MO-MSAR), and from MSAR to movement termination (interval MSAR-MT). Considering that DBS OFF and OL-DBS settings do not have a ramp-up interval, for comparison across the different DBS settings (DBS OFF, OL-DBS, CL-DBS), we used the MO-MSAR interval from the CL-DBS executed during the same month. If no CL-DBS was recorded during that month, we used the patient-matched MO-MSAR average. Similar to what is shown for the tremor amplitude during the whole movement period, during the MSAR-MT interval there was a clear decrease (improvement) of OL-DBS (mixed model ANOVA with patient as random effect, $F_{1,29}=7.4617$, $P=0.0106$) and CL-DBS (mixed model ANOVA with patient as random effect, $F_{1,23}=5.6956$, $P=0.0256$) compared to DBS OFF for all 3 patients (Fig. 4D bottom). The tremor amplitude percent decrease from DBS OFF was -39.0 (SD= 28.4) % for OL-DBS, whereas for CL-DBS was -39.9 (SD= 26.5) %. However, during the MO-MSAR interval the tremor amplitude had a more modest decrease from DBS OFF (Fig. 4D top), with -17.5 (SD= 36.9) % for OL-DBS (mixed model ANOVA with patients as random effect, $F_{1,29}=1.4196$, $P=0.2431$), whereas for CL-DBS was -19.6 (SD= 24.9) % (mixed model ANOVA with patients as random effect, $F_{1,23}=1.9517$, $P=0.1757$). Neither of the DBS settings (OL-DBS and CL-DBS) led to differences from DBS OFF during the MO-MSAR interval, leading to the consideration that there is a brief leftover tremor at every initial movement regardless of the stimulation paradigm.

Longitudinal performance of the fully embedded closed-loop DBS paradigm

The performance of the closed-loop algorithm was evaluated in the fully embedded system by comparing the stimulation delivery with most tremor-affected arm movement (contralateral limb to the implant, based on acceleration traces) and obtaining accuracy, sensitivity, and specificity measures. Figure 5 demonstrates the implementation of the closed-loop paradigm in a single subject in a volitional reaching task (ET01, 3rd month), in which the patient simulated a typical upper extremity movement consisting of reaching and bringing a cup towards themselves. The power in the LFO range was used to detect movement onset and termination (for this recording were set with 15 Hz and 25 Hz as center frequency and 5Hz of bandwidth each), actuating the stimulation delivery (Fig. 5 bottom row). Stimulation did not impede the detection of movement onset and end, as the artifact leakage did not affect the spectral band of interest (LFO) in M1 (Fig. S3). During the volitional cup reaching task, the detection performance in all patients across months showed high accuracy (92.55% [SD=5.23%]), sensitivity (94.17% [SD=8.28%]), specificity (90.99% [SD=5.26%]) and precision (90.61% [SD=7.41%]). The longitudinal patient-specific performance is given in Figures 6A, S4; average patient-specific performance in Figure 6B; overall performance across patients in Figure 6C. A single-task comparison of the therapeutic performance between DBS OFF, CL-DBS, and OL-DBS is shown for each patient (Movie S1: ET01 executing a volitional cup reaching task; Movie S2: ET02 executing a cued-go cup reaching task; Movie S3: ET03 executing a volitional cup reaching task). EMG and inertial

sensors were used only for labeling and tremor evaluations, not as inputs for the control algorithm. Furthermore, the interval MO-SO showed different performances in how early the detector triggered stimulation with respect to movement onset (Fig. 6D), with an average delay of -0.23 (SD=1.21) s across patients. Specifically, for each patient, the MO-SO was: ET01: -0.76 [SD=1.38] s; ET02: -0.22 [SD=1.25] s; ET03: 0.26 [SD=0.79] s). The interval MO-MSAR is further dependent on the ramp-up time of stimulation (max amplitude [V] divided by ramp-up [V/s]) set for each patient at each month, leading to an average delay from MO to MSAR of 1.72 (SD=1.15) s across patients (ET01: 1.13 [SD=1.36] s; ET02: 2.08 [SD=1.13] s; ET03: 1.95 [SD=0.70] s).

Energy savings of closed-loop DBS

We evaluated the energy savings for the proposed closed-loop stimulation paradigm during both in-clinic testing and at home (between two consecutive daily clinic visits, from the afternoon to the morning of the next day), during a typical daily real-life usage (labeled as short-term daily usage). The total electrical energy delivered (TEED) (38) was computed for both OL-DBS and CL-DBS conditions. TEEDs are normalized to the duration of the task, to avoid bias due to each task length (Supplementary Materials and Methods: Classification performance and energy consumption). The energy saving is obtained by comparing the TEED for CL-DBS with the maximum TEED possible with CL-DBS settings (considering CL-DBS always in detect state, leading to CL-DBS being always at the maximum stimulation amplitude possible). The maximum TEED for CL-DBS is equivalent to the TEED of an open-loop paradigm which uses the same DBS parameters of CL-DBS. The mean energy saving for CL-DBS was 57.98% (SD=14.12%) during the clinic testing (Fig. 6E left), and 50.15% (SD=11.47%) while at home (Fig. 6E right). Taking into consideration both clinical effectiveness and energy savings, the results revealed equal clinical benefit for less energy consumption (Fig. 6F), as shown by the TEED (considered as percent difference from the same month OL-DBS TEED), with mixed model ANOVA revealing a main effect of DBS type (OL-DBS vs. CL-DBS) ($F_{1,21}=39.63$, $P=0.000003$) but not for TRS ($F_{1,21}=3.224e-29$, $P=1.000$) (Fig. S5, 6F). Post-hoc testing identified a significant reduction in TEED with respect to DBS type ($t_9=12.89$, $P=4.189e-07$). Comparing CL-DBS TEED to the OL-DBS TEED, taking in consideration the reduction in stimulation parameters (such as pulse width) needed for paresthesia avoidance during CL-DBS (stimulation ramp-up), the mean energy saving improved to 67.93% (SD=16.67%) within clinic testing (monthly percent energy usage Fig. S6A, group energy saving S6B left), and 62.67% (SD=14.26%) while at home (Fig. S6B right). For completeness, there is an estimated extra 10% in power consumption due to the internal event detector (Nexus-E) and sensing circuitry (28, 29, 39), compared to the OL-DBS condition. Nonetheless, one of the benefits of energy savings is the crucial increase in battery life, ultimately reducing battery replacement surgeries. Even considering that new battery chemistries and recharging capabilities are being added to the new generation of neurostimulators, the systems will still benefit from a reduced power consumption due to CL-DBS, decreasing the number of needed re-charges and decreasing the burden on the patient (40).

Longitudinal stability of CL-DBS (6 months)

A critical component of a closed-loop system is a chronically stable control feature. Our study showed the repeatability of a CL-DBS paradigm across 3-4 months. Table S2 shows that the CL-DBS algorithm required retraining only in one instance, for ET01 at month 6, as the change in therapeutic stimulation frequency as identified by a clinician (usage of 180 Hz stimulation)

altered the feature space used previously (due to stimulation subharmonic artifacts). In addition, the maximum LFO decreases during contralateral movement initiation and termination (group PSD average in Fig. S7A, individual PSD LFO drop in Fig. S7B) did not exhibit a statistically significant trend over time (mixed model ANOVA with un-normalized PSD LFO bin, main effect of time, $F_{5,11}=0.49540$, $P=0.7736$). The drift of the LFO maximum decrease during contralateral movement was 1.85 (SD=0.97) dB/month, which we considered being within an acceptable range, similar to a previous study which included subdural strips (41). Additionally, we observed that the feature was not correlated ($R^2=0.0427$, $P=0.4262$) to the impedance over the recording contacts (Fig. S7C) considering the 12.35 (SD=9.01) %/month drift in impedance over time (mixed model ANOVA, main effect of time, $F_{5,11}=7.8007$, $P=0.0023$) (Fig. S7D). However, impedance and power are likely to stabilize over time, as reported in previous studies with long-term cortical implants (42–44). In addition, the CL-DBS detector did not trigger stimulation during other non-movement actions, such as speech. This is shown through a speech execution task with CL-DBS detector active, in which the patient switched between talking and rest periods without eliciting stimulation delivery (Fig. S8A, single subject). The power deviations in the CL feature bands during speech were not sufficient to elicit the delivery of full therapeutic stimulation (Fig. S8B). This helped avoid undesirable stimulation induced side effects.

Patient reporting for CL-DBS usage

No detectable difference between CL-DBS and OL-DBS settings (in tremor suppression performance) were reported by the patients. ET02 also self-reported benefit from CL-DBS related to the decreased incidence of DBS-induced speech impairment. ET03 preferred to use the CL-DBS commenting that the algorithm was well-tuned for his use, whereas ET01 expressed no preference. In addition, although subjects were advised to switch off CL-DBS while sleeping, between the consecutive daily visits at each month, frequently they did not disable CL-DBS. Nonetheless, they did not report any adverse effects or any trouble while sleeping (Table S3). Due to device memory limitations, we were not able to record data while the patients were asleep. Hence, we report that the use of CL-DBS does not add unexpected adverse events during the time it was deployed (between consecutive daily visits at each month).

Discussion

This study demonstrates the feasibility and implementation of closed-loop stimulation for patients affected by ET used in a fully embedded system both in-clinic and at-home environments. The proposed paradigm for stimulation delivery used M1 as a driver for the DBS controller, achieving tremor suppression during movement in three patients. Consequently, it achieved integration with the patient behavior, a feature that is still lacking in currently commercially available DBS devices. Considering that the subset of the patient population enrolled in this study presented tremor mainly when moving, with the movement onset preceding the tremor onset, the movement biomarker was considered sufficient to target such pathological manifestation and facilitated DBS actuation in a timely manner prior to the manifestation of tremor. Tremor-specific features should be further explored; however, for our patient sample with intention tremor, movement-based features provided a reliable and tolerable control policy with rapid stimulation delivery that overcame stimulation artifact issues.

Our data, along with other recent studies (45–50) showed it is possible to directly use the VIM to detect movement and tremor features. However, the stimulation would adversely affect recording

quality, especially when delivering stimulation to contacts adjacent to the recording site, rendering the detection of the termination of movement/tremor impossible. In addition, other studies used external amplifiers connected to externalized electrodes or to single-unit recordings setups with a more favorable signal to noise ratios, which have power consumption and form factors currently beyond what is feasible in the available implantable systems, considering that the DBS implants require considerable longevity to avoid to battery replacement surgeries (29). Newer platforms are under development to address this shortcoming (51). Including a non-target DBS area for the sensing (from M1) placed fewer constraints on the stimulation parameter space, avoiding the interdependence of stimulation and sensing contacts (bipolar sensing with symmetric contacts around a single contact used for monopolar stimulation). Nonetheless, our paradigm required the insertion of an additional subdural strip over the motor cortex, which had no previously known clinical benefit in an OL-DBS scenario and is not part of the usual standard of care. However, it required little to no variation to the standard DBS implantation surgery, using similar surgical constraints to the DBS lead targeting. The placement can be performed at the same time as the DBS lead implantation through the same burr-hole, and it has currently not been associated with adverse outcomes when used in our long term studies (41) and within other groups performing similar implants (39, 52, 53). Although other prior studies used a similar stimulation delivery approach based on cortical detection, they required the presence of an external controller (computer-in-the-loop with a telemetry wand) and lacked a longer-term evaluation of the paradigm during a realistic daily life scenario (in the clinic and at home) (54).

As onset of stimulation may commonly cause paresthesia in open-loop approaches, we had to optimize CL-DBS for tolerability. Although a slower ramp-up of stimulation amplitude improved tolerability, we also aimed to initiate therapeutic stimulation prior to tremor manifestation. Since movement preceded the tremor onset, our embedded classifier was able to initiate DBS with an optimized slope that could suppress tremor and avoid paresthesia. Importantly, the closed-loop DBS users had a good response to the proposed stimulation paradigm. Tremor increased at the beginning of the movement, independent of the timing of stimulation delivery (DBS OFF, OL-DBS and CL-DBS). As shown in Figure 4D, this is not bounded to the CL-DBS setup, but is a problem also present in OL-DBS. Nonetheless, considering the shortness of the interval of interest (MO-MSAR, 1.72 [SD=1.15] s), the modest decrease in tremor amplitude compared to DBS OFF, seems sufficient to not create discomfort to the subject while executing a movement, as reported in previous OL-DBS studies (3, 24). Analysis of the total energy delivered (TEED) during CL-DBS was shown to be lower compared to OL-DBS. The blinded clinical scores (TRS) and tremor amplitude showed equal effectiveness for both DBS settings (OL-DBS and CL-DBS).

Preliminary findings on other clinical benefits of closed-loop DBS seem to indicate that this stimulation paradigm can help address DBS-induced impairment, as it delivered DBS only when the patient presented tremor-related movement. The timing of DBS in response to patient symptoms is an important driver for the reduction of side effects. The reduction of DBS parameters (amplitude, pulse width, frequency) can also contribute to the reduction of side effects, but it is only beneficial if it maintains the same therapeutic benefit, as shown in our data. In addition, due to the lack of unexpected adverse events during the deployment of this paradigm, including the cases where CL-DBS was left active during sleep, we conclude that CL-DBS appears to be safely implementable. Further out-of-clinic testing (daily life scenarios) will be pursued in the next phase of this study.

We observed that cortical placement was an important factor in our paradigm. As such, we assumed ET02 had the worst performance with an accuracy of 85.90% (SD=4.71%), and sensitivity 83.86% (SD=10.57%) out of the three subjects because of a less than optimal cortical placement, as only a single contact was above the precentral gyrus and consequently all bipolar combinations included non-M1 areas. The cause behind the suboptimal placement can be found in the surgical avoidance of conspicuous blood vessels.

Limitations in this study included restrictions for the classification algorithm, which was limited to the implementation of a simple linear classifier (see Materials and Methods: Embedded classification and debugging) with a single threshold control strategy, which in the future could be expanded in second generation bidirectional neurostimulators with more flexibility (55). A wider set of features and advanced algorithms could increase the performance for the actuation of closed-loop DBS. Moreover, current device limitations did not allow reliable detection of broadband high gamma (BHG) activity from the power estimators used by the embedded detector. BHG activity modulates the most during contralateral movement and is more local (56–59). We expect that improved device noise floor would enable the use of BHG features for more reliable movement detection (55), leading to a more stable MO-SO interval across patients, and avoiding to trigger stimulation during ipsilateral movement. However, we argue that being able to detect and stimulate for both ipsi- and contralateral movement from a single location could be beneficial, as it requires only one side for cortical implantation, and previous studies have shown benefit from ipsilateral stimulation on tremor severity (60, 61). Future studies should evaluate the performances of CL-DBS detection in a wider set of movements, such as walking, to ensure accuracy of stimulation delivery. Hence, considering the locality of BHG (56–59), detection based on BHG features could help address shortcomings of LFO-based detection, such as cross-site activation (feet motor areas). However, we showed that the current LFO-based detection was able to avoid spurious detection during speech, even considering the proximity of hand-motor areas to face related areas (62). Additional limitations of this study were the limited sample size (3 patients), the focus on detection only during upper limb movements, and the lack of quantitative measures of side effects such as speech impairment. Larger longitudinal studies are needed to account for the quantification of efficacy and side effects, together with testing a wider set of movements in real-life scenarios, such as reaching for objects while walking. Improvements in neurostimulators are now in development, which could enable further detection capabilities and at-home testing scenarios (55). Furthermore, this study addresses the tremor manifestation during limb movement, and does not address tremor manifesting in the head, neck, and voice.

Our goal for this study was to demonstrate the stability of a movement-based CL-DBS over time. This approach has considerably lower energy delivery, delivering stimulation only when needed, while maintaining clinical effectiveness in a range of movements (cup reaching, proximal and distal posture, water pouring, writing). The proposed paradigm is a first step towards behaviorally modulated fully embedded DBS systems (63). This strategy requires an additional clinical step for the programming of the responsiveness of the controller. However, we note that the training sessions required little to no effort, as the system was using simple tasks. In summary, this work illustrates a comprehensive strategy for the training and deployment of closed-loop DBS therapies that are completely embedded within the patient's body, are responsive to real-time patient behavior, and integrate seamlessly with daily life activities.

Materials and Methods

Study Design

The aim of this study was to show the feasibility and implementation of a self-adjusting therapeutic DBS for patients affected by ET, based on motor behavior detection.

Neurological data were collected from M1 and VIM from the Activa PC+S neurostimulator over six monthly visits post-surgery in 3 patients affected by ET. Blinded-raters scored patients' clinical outcomes (Tremor Rating Scale, TRS) in an in-subject crossover protocol (DBS OFF, OL-DBS, CL-DBS). The patient was blinded to which setting was being tested during the clinical evaluation (TRS). No randomization was present in this study, as all patients were being tested in all three conditions (DBS OFF, OL-DBS, CL-DBS). Subjects were enrolled in our study if they qualified within the inclusion and exclusion criteria as reported at Clinicaltrials.gov: NCT02649166. No patients were excluded after implantation of the Activa PC+S. Enrollment inclusion and exclusion criteria are reported in the Supplementary Materials and Methods: Selection criteria section. Sample sizes were derived from patient availability and feasibility of enrollment at the University of Florida. Moreover, the study is sized appropriately for a feasibility pilot study, with neurotechnology being explored for the proposed application space. The subject numbers are consistent with published reports in the literature for DBS including recent examples from depression (64), obsessive compulsive disorder (65), and Tourette's syndrome (66). The sample size is also in line with regulatory expectations (FDA) for pilot feasibility efforts. The first month was dedicated to integrating information from anatomical images and intra-operative recordings for assessing the best contacts for data acquisition. Initial testing revealed that bipolar stimulation of VIM caused the least amount of stimulation artifact in the cortical channel (Fig. S2).

Participants

We received FDA and University of Florida Institutional Review Board (IRB) approval (ET Closed Loop DBS Study, ClinicalTrials.gov: NCT02649166) for a closed-loop DBS study to treat 10 patients with medically refractory ET using Medtronic Activa PC+S neurostimulators (27). To date, we enrolled 3 patients at the University of Florida Norman Fixel Institute for Neurological Diseases (Table S1).

Experimental Task Design

The subjects performed 5 tasks: (i) Baseline, in which the subject was asked to remain still in a resting position, without contracting muscles to maintain any posture; (ii) Cued-go hand opening and closing, in which the subject was cued to open and close their left or right hand in a random order. When cued the subject had to prepare to move with a specific hand (CUE, for 1.5 ± 0.5 seconds). Next, the subject was cued for how long to perform the movement (GO CUE, for 6.5 ± 0.5 seconds). Each moving phase was stopped by a rest cue, where the subject returned to the resting position used during the baseline task for 6.5 ± 1.5 seconds (Fig. 3A top); (iii) Cued-go cup reaching, in which the subject was asked to reach a cup, bring it towards their mouth and bring it back to the hand of the operator/researcher, in the original position. Only one hand was used at a time. The subject was cued to prepare to reach the cup with a specific hand CUE, for 2 ± 1 seconds), requiring no actual movement during this phase, and then a second cue (GO CUE) indicated to initiate the movement (Fig. 3A bottom). Between the GO CUE and the next CUE there was an interval of 12 ± 2 seconds. In addition, the patient had to simulate the drinking action with the cup, by bringing it towards themselves, next to their mouth, and back to the original position to evoke tremor; (iv) Self-initiated cup reaching, in which the subject executed

the previous task without being cued for which hand to use and when the movement had to start. The rest interval was also self-selected by the subject; (v) Postural tremor task (block= \sim 20s; 3 times distal posture, 3 times proximal posture, randomized; ISI=20s). Tasks were executed with and without DBS. When cups were used, they were filled with water to evoke tremor. Local field potentials (LFPs) were acquired at 793.6 and 422 Hz in standalone mode (hardware lowpass at 100 Hz) with power channels disabled, unless a close-loop testing was in progress (with Nexus E). Electromyography (EMG)/Inertia (accelerometer, gyroscope, and magnetometer) data were acquired respectively at 1000 Hz and 148.25 Hz (Trigno Wireless EMG, Delsys). The EMG/Inertia sensors were placed on the patients' upper limbs (hand dorsum, flexor carpi ulnaris, bicep on both arms) to detect movement onset/tremor. Video data were acquired at 24 Hz to capture behavioral activity. All the sources but the PC+S were aligned with a train of square pulses ("sync trigger") delivered to a dedicated shared channel, expanded from the setup used in previous work (33). The alignment of the neural data collected with the Activa PC+S with EMG (and therefore the other sources), was achieved by delivering a short stimulation burst (\sim 2 s) at 5 Hz. The stimulation termination could be detected both in the DBS lead and in the EMG positioned near the neck, where the DBS extension cable was passing. The alignment was executed at the beginning of each run execution. Once we had viable features for movement detection, at the third month we proceeded to program and to optimize the closed-loop DBS implementation. In addition, we currently are seeking approval for letting the patients use the embedded CL-DBS system at home, between the monthly visits.

DBS Programming, Clinical Evaluation, and Short-term Daily Real-life Usage

The patients underwent DBS programming as standard clinical care, optimizing the effectiveness of the stimulation to suppress the symptoms. The same clinical setting for open-loop stimulation was used as basis for closed-loop programming. Often the closed-loop stimulation parameters had to be reduced to prevent paresthesia due to a fast stimulation onset, which was mild in intensity but could lead to discomfort. The Fahn-Tolosa-Marin TRS was used for clinical evaluation (34). The off-DBS, open- and closed-loop DBS effects on tremor and hand function were assessed at every follow-up visit. The neurologist and patient were blinded to avoid bias. Furthermore, CL-DBS energy saving was also evaluated during a typical daily real-life usage (labeled as short-term daily usage), in the time between two consecutive daily visits, from the afternoon to the morning of the next day. As we could not directly measure the tremor outside the clinic, we could only estimate energy usage based on the detection, stimulation and neural features logs. We also relied on the patient feedback to know if the paradigm tested was effective in suppressing their tremor when at home (during the short-term daily usage).

Signal Processing of Neural Signals and Accelerometer Data

All analyses were executed within the MATLAB 2018a environment (MathWorks) with custom scripts. Medtronic provided libraries to enable interfacing with the Activa PC+S neurostimulator.

As a first preprocessing step, the recorded channels (two bipolar configurations, 1 cortical and 1 thalamic) were inspected for artifacts and signal quality through visual inspection of the raw time series, the power spectral densities (PSD) across tasks, and the spectrograms. An additional high-pass filter at 1Hz was used to eliminate the time series drift and to reject low frequency device-noise. No channels were dropped from the subsequent analyses. PSDs and spectrograms were computed by using an autoregressive model (67, 68) with a frequency resolution of 1 Hz.

Accelerometer data were analyzed for tremor amplitude quantification, by using the most distal sensors (hands). The tremor amplitude was computed by calculating the triaxial magnitude of the accelerometer amplitude profiles. The data were band-passed at the tremor frequency, using a Hilbert transform to obtain the amplitude envelope for each axis before point by point magnitude calculation. The tremor frequency was selected by looking at the frequency with a clear peak in power in the PSD in the presence of tremor symptoms.

Embedded classification and debugging

The onboard classifier of the Activa PC+S implanted neurostimulator was programmed based on an LDA algorithm, the only available embedded classifier, which takes up to two power bands specified a priori as inputs. The system allows for the selection of the center frequency and bandwidth for the calculation of one power band (minimum bandwidth was 5 Hz). These power channels are based on analog power estimators sampled with 10bit ADCs, which are separate from the ADC used to sample the raw trace (27, 29, 51). Hence, offline training based only on spectral estimation of the power channels from the time-series signal yielded unreliable results when used to directly obtain the weights for the embedded LDA algorithm. In addition, the stimulation affected the power channels when active, leading to a variety of effects such as saturation (with unrecoverable neuromarkers), major artifacts (with unrecoverable neuromarkers, as in Fig. S1), minor artifacts (with recoverable neuromarkers, as in Fig. S2, 5, and S3). Many combinations of power settings and DBS settings could lead to power modulation (power increase) when stimulation was delivered, increasing the risk of going over the detection threshold and possibly causing a continuous toggling between stim-on/stim-off state (Fig. S9). The Medtronic Activa PC+S device is enabled for onboard logging of additional information and internal states together with the neural activity, such as the detection status (detection True/False). To verify accurate stimulation delivery, we filtered the cortical activity with a bandpass filter centered around the stimulation frequency (Fig S10). We chose to compute the estimate of the delivered stimulation using the detection state (internal LDA) and the neurostimulator parameters (amplitude, ramp-up time, ramp-down time, detection onset delay, detection termination delay), leading to a cleaner trace. Its reliability was tested by comparing the two estimates (Fig. S10).

Risk and Mitigations

The deployment of the system in a complex scenario, taking in consideration a large variety of potential issues and pitfalls, required the presence of safety mechanisms for the protection of the patient. A possible case would be when there could be a failure of the sensing stage of the implanted neurostimulator. Other case scenarios were stimulation artifact and edge cases which cause stimulation toggling (Fig. S9), which could be possibly encountered due to progressive drift of the acquisition stage (power estimates) over time. To that end, a fallback “safe” mode (30) was provided to the subject, which was quickly available by using the provided patient programmer. In our cohort we did not encounter any device failures. The role of this mode was to quickly provide a clinically approved stimulation state, to deliver a therapeutic DBS with no interruption to the patient benefit.

Statistical analyses

MATLAB statistical package was used (R2018a). Data were tested for normal (Gaussian) distribution using Shapiro-Wilk normality test. All correlation are Pearson and all p-values are two-tailed, except in the TOST procedure (69, 70). A p-value < 0.05 was considered statistically

significant (p-value is specified). In addition, each statistic technique used is mentioned individually within the results section. Repeated measures were tested with a mixed model ANOVA. Specifically, we used the subsequent models for each of these results: TRS deviation from DBS OFF for CL-DBS and OL-DBS, mixed model ANOVA with patient as random effect “ $\text{TRS_score} \sim \text{DBS_type} + (1|\text{pat_id})$ ”; amplitude change from DBS OFF for CL-DBS and OL-DBS, mixed model ANOVA with patient as random effect “ $\text{acceleration_amplitude} \sim \text{DBS_type} + (1|\text{pat_id})$ ”; the same model was used for the MO-MSAR and MSAR-MT accelerations amplitudes; energy saving evaluation based on TEED comparisons across different stimulation settings (DBS OFF, OL-DBS, CL-DBS), mixed model ANOVA with patient as random effect “ $\text{TEED} \sim \text{TRS_score} * \text{DBS_type} + (1|\text{pat_id})$ ”; PSD stability over time was evaluated with a mixed model ANOVA with patient as random effect “ $\text{power_LFO} \sim \text{months} + (1|\text{pat_id})$ ”; impedance stability over time was evaluated with a mixed model ANOVA with patient as random effect “ $\text{impedance} \sim \text{month} + (1|\text{pat_id})$ ”.

Supplementary Materials

Materials and Methods

Fig. S1. Artifacts from stimulation impaired data collection from VIM contacts.

Fig. S2. Artifacts from stimulation did not impair movement detection performances from cortical contacts.

Fig. S3. Implementation of closed-loop DBS in a patient affected by ET showing spectral leakage of the stimulation artifact.

Fig. S4. Performances of the embedded detector over the monthly clinical/research visit in all the enrolled subjects.

Fig. S5. TRS improvements vs TEED savings in percent.

Fig. S6. Energy performance of closed-loop DBS at monthly visits in all the enrolled subjects compared to open-loop DBS energy consumption (TEED).

Fig. S7. PSD and impedance over 6 months period.

Fig. S8. Performance of closed-loop DBS in patients affected by ET during speech execution.

Fig. S9. Example of a non-optimized embedded closed-loop stimulation paradigm.

Fig. S10. Stimulation delivery estimated by two different methodologies.

Table S1. Subject demographics for the study.

Table S2. DBS and closed-loop settings at each month for each patient during TRS clinical evaluation.

Table S3. DBS related side effects reported.

Data File S1. Data for Figures 2-6, and Supplementary Figure S3, S4, S6.

Data File S2. Data for Supplementary Figures S1-S2, S5, S7-S10.

Movie S1. Comparison between DBS OFF, closed-loop DBS (fully embedded implementation), and open-loop DBS in ET01 during a volitional movement task.

Movie S2. Comparison between DBS OFF, closed-loop DBS (fully embedded implementation), and open-loop DBS in ET02 during a cued-go cup reaching task.

Movie S3. Comparison between DBS OFF, closed-loop DBS (fully embedded implementation), and open-loop DBS in ET03 during a volitional cup reaching task.

References and Notes:

1. J. A. Semrau, T. M. Herter, Z. H. Kiss, S. P. Dukelow, Disruption in proprioception from long-term thalamic deep brain stimulation: a pilot study, *Front. Hum. Neurosci.* **9** (2015), doi:10.3389/fnhum.2015.00244.
2. D. Mücke, J. Becker, M. T. Barbe, I. Meister, L. Liebhart, T. B. Roettger, T. Dembek, L. Timmermann, M. Grice, The Effect of Deep Brain Stimulation on the Speech Motor System, *J. Speech Lang. Hear. Res.* **57**, 1206 (2014).
3. T. A. Zesiewicz, J. D. Shaw, K. G. Allison, J. S. Staffetti, M. S. Okun, K. L. Sullivan, Update on treatment of essential tremor, *Curr. Treat. Options Neurol.* **15**, 410–423 (2013).
4. D. Mücke, A. Hermes, T. B. Roettger, J. Becker, H. Niemann, T. A. Dembek, L. Timmermann, V. Visser-Vandewalle, G. R. Fink, M. Grice, M. T. Barbe, P. Gonzalez-Alegre, Ed. The effects of Thalamic Deep Brain Stimulation on speech dynamics in patients with Essential Tremor: An articulographic study, *PLoS One* **13**, e0191359 (2018).
5. K. T. Mitchell, P. Larson, P. A. Starr, M. S. Okun, R. E. Wharen, R. J. Uitti, B. L. Guthrie, D. Peichel, R. Pahwa, H. C. Walker, K. Foote, F. J. Marshall, J. Jankovic, R. Simpson, F. Phibbs, J. S. Neimat, R. M. Stewart, K. Dashtipour, J. L. Ostrem, Benefits and risks of unilateral and bilateral ventral intermediate nucleus deep brain stimulation for axial essential tremor symptoms, *Parkinsonism Relat. Disord.* **60**, 126–132 (2019).
6. J. G. Pilitsis, L. V. Metman, J. R. Toleikis, L. E. Hughes, S. B. Sani, R. A. E. Bakay, Factors involved in long-term efficacy of deep brain stimulation of the thalamus for essential tremor, *J. Neurosurg. Pediatr.* **109**, 640–646 (2008).
7. C. G. Favilla, D. Ullman, A. Wagle Shukla, K. D. Foote, C. E. Jacobson, M. S. Okun, Worsening essential tremor following deep brain stimulation: disease progression versus tolerance, *Brain* **135**, 1455–1462 (2012).
8. M. J. Birdno, A. M. Kuncel, A. D. Dorval, D. A. Turner, R. E. Gross, W. M. Grill, Stimulus features underlying reduced tremor suppression with temporally patterned deep brain stimulation, *J. Neurophysiol.* **107**, 364–383 (2012).
9. E. D. Louis, R. Ottman, How many people in the USA have essential tremor? Deriving a population estimate based on epidemiological data., *Tremor Other Hyperkinet. Mov. (N. Y.)* **4**, 259 (2014).
10. E. D. Louis, J. J. Ferreira, How common is the most common adult movement disorder? Update on the worldwide prevalence of essential tremor, *Mov. Disord.* **25**, 534–541 (2010).
11. E. D. Louis, L. Barnes, S. M. Albert, L. Cote, F. R. Schneier, S. L. Pulman, Q. Yu, Correlates of functional disability in essential tremor, *Mov. Disord.* **16**, 914–920 (2001).
12. S. P. Woods, J. C. Scott, J. A. Fields, A. Poquette, A. I. Tröster, Executive dysfunction and

neuropsychiatric symptoms predict lower health status in essential tremor., *Cogn. Behav. Neurol.* **21**, 28–33 (2008).

13. D. Lorenz, D. Schwieger, H. Moises, G. Deuschl, Quality of life and personality in essential tremor patients, *Mov. Disord.* **21**, 1114–1118 (2006).

14. F. R. Schneier, L. F. Barnes, S. M. Albert, E. D. Louis, Characteristics of Social Phobia Among Persons With Essential Tremor, *J. Clin. Psychiatry* **62**, 367–372 (2001).

15. K. P. Bhatia, P. Bain, N. Bajaj, R. J. Elble, M. Hallett, E. D. Louis, J. Raethjen, M. Stamelou, C. M. Testa, G. Deuschl, Consensus Statement on the classification of tremors. from the task force on tremor of the International Parkinson and Movement Disorder Society, *Mov. Disord.* **33**, 75–87 (2018).

16. G. Deuschl, Essential tremor and cerebellar dysfunction Clinical and kinematic analysis of intention tremor, *Brain* **123**, 1568–1580 (2000).

17. P. Feys, W. Helsen, A. Lavrysen, B. Nuttin, P. Ketelaer, Intention tremor during manual aiming: a study of eye and hand movements, *Mult. Scler.* **9**, 44–54 (2003).

18. W. J. Elias, B. B. Shah, Tremor, *JAMA* **311**, 948–954 (2014).

19. E. D. Louis, E. Rios, C. Henchcliffe, How Are We Doing With the Treatment of Essential Tremor (ET)? Persistence of Patients With ET on Medication: Data From 528 Patients in Three Settings, *Eur. J. Neurol.* **17**, 882–884 (2010).

20. M. F. Brin, K. E. Lyons, J. Doucette, C. H. Adler, J. N. Caviness, C. L. Comella, R. M. Dubinsky, J. H. Friedman, B. V. Manyam, J. Y. Matsumoto, S. L. Pullman, A. H. Rajput, K. D. Sethi, C. Tanner, W. C. Koller, A randomized, double masked, controlled trial of botulinum toxin type A in essential hand tremor, *Neurology* **56**, 1523–1528 (2001).

21. V. Castrillo-Fraile, E. C. Peña, J. M. T. Gabriel Y Galán, P. D. Delgado-López, C. Collazo, E. Cubo, Tremor Control Devices for Essential Tremor: A Systematic Literature Review *Tremor Other Hyperkinet. Mov. (N. Y.)* **9** (2019), doi:10.7916/tohm.v0.688.

22. J. Á. Gallego, J. Ibáñez, J. L. Dideriksen, J. I. Serrano, M. D. Del Castillo, D. Farina, E. Rocon, A multimodal human-robot interface to drive a neuroprosthesis for tremor management, *IEEE Trans. Syst. Man Cybern. Part C Appl. Rev.* **42**, 1159–1168 (2012).

23. F. B. Nahab, E. Peckham, M. Hallett, Essential tremor, deceptively simple ..., *Pract. Neurol.* **7**, 222–233 (2007).

24. A. Chopra, B. T. Klassen, M. Stead, Current clinical application of deep-brain stimulation for essential tremor, *Neuropsychiatr. Dis. Treat.* **9**, 1859–1865 (2013).

25. J. a Brodkey, R. R. Tasker, C. Hamani, M. P. McAndrews, J. O. Dostrovsky, A. M. Lozano, Tremor cells in the human thalamus: differences among neurological disorders., *J. Neurosurg.* **101**, 43–47 (2004).

26. P. Khanna, S. Stanslaski, Y. Xiao, T. Ahrens, D. Bourget, N. Swann, P. Starr, J. M. Carmena, T. Denison, in *IEEE Biomedical Circuits and Systems Conference: Engineering for Healthy Minds and Able Bodies, BioCAS 2015 - Proceedings*, (Institute of Electrical and Electronics Engineers Inc., 2015), pp. 1–6.

27. S. Stanslaski, P. Afshar, P. Cong, J. Giftakis, P. Stypulkowski, D. Carlson, D. Linde, D.

- Ullestad, A. T. Avestruz, T. Denison, Design and validation of a fully implantable, chronic, closed-loop neuromodulation device with concurrent sensing and stimulation, *IEEE Trans. Neural Syst. Rehabil. Eng.* **20**, 410–421 (2012).
28. P. Afshar, A. Khambhati, S. Stanslaski, D. Carlson, R. Jensen, D. Linde, S. Dani, M. Lazarewicz, P. Cong, J. Giftakis, P. Stypulkowski, T. Denison, A translational platform for prototyping closed-loop neuromodulation systems., *Front. Neural Circuits* **6**, 117 (2012).
29. A.-T. Avestruz, W. Santa, D. Carlson, R. Jensen, S. Stanslaski, A. Helfenstine, T. Denison, A 5 μ W/Channel Spectral Analysis IC for Chronic Bidirectional Brain-Machine Interfaces, *IEEE J. Solid-State Circuits* **43**, 3006–3024 (2008).
30. A. Gunduz, E. Opri, R. Gilron, V. Kremen, G. Worrell, P. Starr, K. Leyde, T. Denison, Adding wisdom to ‘smart’ bioelectronic systems: a design framework for physiologic control including practical examples, *Bioelectron. Med.* **2**, 29–41 (2019).
31. C. R. Butson, S. E. Cooper, J. M. Henderson, C. C. McIntyre, Patient-specific analysis of the volume of tissue activated during deep brain stimulation., *Neuroimage* **34**, 661–70 (2007).
32. C. Choe, U. Hidding, M. Schaper, A. Gulberti, J. Köppen, C. Buhmann, C. Gerloff, C. K. E. Moll, W. Hamel, M. Pötter-Nerger, Thalamic short pulse stimulation diminishes adverse effects in essential tremor patients, *Neurology* **91**, e704–e713 (2018).
33. E. Opri, S. Cernera, M. S. Okun, K. D. Foote, A. Gunduz, The Functional Role of Thalamocortical Coupling in the Human Motor Network, *J. Neurosci.* , 1153–19 (2019).
34. S. Fahn, E. Tolosa, M. Concepcion, in *Parkinson’s disease and movement disorders*, J. Jankovic, E. Tolosa, Eds. (Williams and Wilkins, Baltimore, 1993), pp. 271–280.
35. M. A. Stacy, R. J. Elble, W. G. Ondo, S. C. Wu, J. Hulihan, Assessment of interrater and intrarater reliability of the Fahn-Tolosa-Marin Tremor Rating Scale in essential tremor, *Mov. Disord.* **22**, 833–838 (2007).
36. H. Cagnan, J. S. Brittain, S. Little, T. Foltynie, P. Limousin, L. Zrinzo, M. Hariz, C. Joint, J. Fitzgerald, A. L. Green, T. Aziz, P. Brown, Phase dependent modulation of tremor amplitude in essential tremor through thalamic stimulation, *Brain* **136**, 3062–3075 (2013).
37. H. Cagnan, D. Pedrosa, S. Little, A. Pogosyan, B. Cheeran, T. Aziz, A. Green, J. Fitzgerald, T. Foltynie, P. Limousin, L. Zrinzo, M. Hariz, K. J. Friston, T. Denison, P. Brown, Stimulating at the right time: Phase-specific deep brain stimulation, *Brain* **140**, 132–145 (2017).
38. A. M. Koss, R. L. Alterman, M. Tagliati, J. L. Shils, Calculating total electrical energy delivered by deep brain stimulation systems, *Ann. Neurol.* **58**, 168–168 (2005).
39. N. C. Swann, C. de Hemptinne, M. C. Thompson, S. Miocinovic, A. M. Miller, R. Gilron, J. L. Ostrem, H. J. Chizeck, P. A. Starr, Adaptive deep brain stimulation for Parkinson’s disease using motor cortex sensing., *J. Neural Eng.* **15**, 046006 (2018).
40. T. Khaleeq, H. Hasegawa, M. Samuel, K. Ashkan, Fixed-Life or Rechargeable Battery for Deep Brain Stimulation: Which Do Patients Prefer?, *Neuromodulation Technol. Neural Interface* (2018), doi:10.1111/ner.12810.
41. J. B. Shute, M. S. Okun, E. Opri, R. Molina, P. J. Rossi, D. Martinez-Ramirez, K. D. Foote, A. Gunduz, Thalamocortical network activity enables chronic tic detection in humans with

Tourette syndrome, *NeuroImage Clin.* **12**, 165–172 (2016).

42. K. A. Sillay, P. Rutecki, K. Cicora, G. Worrell, J. Drazkowski, J. J. Shih, A. D. Sharan, M. J. Morrell, J. Williams, B. Wingeier, Long-term measurement of impedance in chronically implanted depth and subdural electrodes during responsive neurostimulation in humans, *Brain Stimul.* **6**, 718–726 (2013).
43. K. A. Sillay, S. Ondoma, B. Wingeier, D. Schomberg, P. Sharma, R. Kumar, G. S. Miranpuri, J. Williams, Long-Term Surface Electrode Impedance Recordings Associated with Gliosis for a Closed-Loop Neurostimulation Device, *Ann. Neurosci.* **25**, 289–298 (2019).
44. F. T. Sun, S. Arcot Desai, T. K. Tcheng, M. J. Morrell, Changes in the electrocorticogram after implantation of intracranial electrodes in humans: The implant effect, *Clin. Neurophysiol.* **129**, 676–686 (2018).
45. H. Tan, J. Debarros, S. He, A. Pogosyan, T. Z. Aziz, Y. Huang, S. Wang, L. Timmermann, V. Visser-Vandewalle, D. J. Pedrosa, A. L. Green, P. Brown, Decoding voluntary movements and postural tremor based on thalamic LFPs as a basis for closed-loop stimulation for essential tremor, *Brain Stimul.* (2019), doi:10.1016/J.BRS.2019.02.011.
46. D. J. Pedrosa, P. Brown, H. Cagnan, V. Visser-Vandewalle, J. Wirths, L. Timmermann, J.-S. Brittain, A functional micro-electrode mapping of ventral thalamus in essential tremor., *Brain* **141**, 2644–2654 (2018).
47. S. E. Hua, F. A. Lenz, Posture-Related Oscillations in Human Cerebellar Thalamus in Essential Tremor Are Enabled by Voluntary Motor Circuits, *J. Neurophysiol.* **93**, 117–127 (2005).
48. A. Kane, W. D. Hutchison, M. Hodaie, A. M. Lozano, J. O. Dostrovsky, Enhanced synchronization of thalamic theta band local field potentials in patients with essential tremor, *Exp. Neurol.* **217**, 171–176 (2009).
49. C. Brücke, A. Bock, J. Huebl, J. K. Krauss, T. Schönecker, G. H. Schneider, P. Brown, A. A. Kühn, Thalamic gamma oscillations correlate with reaction time in a Go/noGo task in patients with essential tremor, *Neuroimage* **75**, 36–45 (2013).
50. S. Little, A. Pogosyan, S. Neal, B. Zavala, L. Zrinzo, M. Hariz, T. Foltynie, P. Limousin, K. Ashkan, J. FitzGerald, A. L. Green, T. Z. Aziz, P. Brown, Adaptive deep brain stimulation in advanced Parkinson disease., *Ann. Neurol.* **74**, 449–57 (2013).
51. S. Stanslaski, J. Herron, T. Chouinard, D. Bourget, B. Isaacson, V. Kremen, E. Opri, W. Drew, B. Brinkmann, A. Gunduz, T. Adamski, G. Worrell, T. Denison, A Chronically-Implanted Neural Coprocessor for Exploring Treatments for Neurological Disorders, *IEEE Trans. Biomed. Circuits Syst.* , 1–1 (2018).
52. N. C. Swann, C. de Hemptinne, S. Miocinovic, S. Qasim, J. L. Ostrem, N. B. Galifianakis, M. S. Luciano, S. S. Wang, N. Ziman, R. Taylor, P. A. Starr, Chronic multisite brain recordings from a totally implantable bidirectional neural interface: experience in 5 patients with Parkinson’s disease., *J. Neurosurg.* **128**, 605–616 (2018).
53. F. Panov, E. Levin, C. de Hemptinne, N. C. Swann, S. Qasim, S. Miocinovic, J. L. Ostrem, P. A. Starr, Intraoperative electrocorticography for physiological research in movement disorders: principles and experience in 200 cases, *J. Neurosurg.* **126**, 122–131 (2017).

54. B. Houston, M. Thompson, A. Ko, H. Chizeck, A machine-learning approach to volitional control of a closed-loop deep brain stimulation system, *J. Neural Eng.* **16**, 016004 (2019).
55. S. Stanslaski, J. Herron, T. Chouinard, D. Bourget, B. Isaacson, V. Kremen, E. Opri, W. Drew, B. H. Brinkmann, A. Gunduz, T. Adamski, G. A. Worrell, T. Denison, A Chronically Implantable Neural Coprocessor for Investigating the Treatment of Neurological Disorders, *IEEE Trans. Biomed. Circuits Syst.* **12** (2018), doi:10.1109/TBCAS.2018.2880148.
56. K. J. Miller, S. Zanos, E. E. Fetz, M. den Nijs, J. G. Ojemann, Decoupling the Cortical Power Spectrum Reveals Real-Time Representation of Individual Finger Movements in Humans, *J. Neurosci.* **29**, 3132–3137 (2009).
57. K. J. Miller, E. C. Leuthardt, G. Schalk, R. P. N. Rao, N. R. Anderson, D. W. Moran, J. W. Miller, J. G. Ojemann, Spectral Changes in Cortical Surface Potentials during Motor Movement, *J. Neurosci.* **27**, 2424–2432 (2007).
58. K. J. Miller, G. Schalk, E. E. Fetz, M. den Nijs, J. G. Ojemann, R. P. N. Rao, Cortical activity during motor execution, motor imagery, and imagery-based online feedback, *Proc. Natl. Acad. Sci.* **107**, 4430–4435 (2010).
59. T. Jiang, N. F. Ince, T. Jiang, T. Wang, S. Mei, Y. Li, X. Wang, Z. Sha, Local spatial correlation analysis of hand flexion/extension using intraoperative high-density ECoG, *Proc. Annu. Int. Conf. IEEE Eng. Med. Biol. Soc. EMBS* **2015-Novem**, 6190–6193 (2015).
60. W. Ondo, K. Dat Vuong, M. Almaguer, J. Jankovic, R. K. Simpson, Thalamic deep brain stimulation: Effects on the nontarget limbs, *Mov. Disord.* **16**, 1137–1142 (2001).
61. Z. Peng-Chen, T. Morishita, D. Vaillancourt, C. Favilla, K. D. Foote, M. S. Okun, A. Wagle Shukla, Unilateral thalamic deep brain stimulation in essential tremor demonstrates long-term ipsilateral effects, *Park. Relat. Disord.* **19**, 1113–1117 (2013).
62. J. Roland, P. Brunner, J. Johnston, G. Schalk, E. C. Leuthardt, Passive real-time identification of speech and motor cortex during an awake craniotomy, *Epilepsy Behav.* **18**, 123–128 (2010).
63. W. J. Neumann, R. S. Turner, B. Blankertz, T. Mitchell, A. A. Kühn, R. M. Richardson, Toward Electrophysiology-Based Intelligent Adaptive Deep Brain Stimulation for Movement Disorders, *Neurotherapeutics* **16**, 105–118 (2019).
64. C. S. Kubu, T. Brelje, M. A. Butters, T. Deckersbach, P. Malloy, P. Moberg, A. I. Tröster, E. Williamson, G. H. Baltuch, M. T. Bhati, L. L. Carpenter, D. D. Dougherty, R. H. Howland, A. R. Rezai, D. A. Malone, Cognitive outcome after ventral capsule/ventral striatum stimulation for treatment-resistant major depression, *J. Neurol. Neurosurg. Psychiatry* **88**, 262–265 (2017).
65. L. Islam, A. Franzini, G. Messina, S. Scarone, O. Gambini, Deep brain stimulation of the nucleus accumbens and bed nucleus of stria terminalis for obsessive-compulsive disorder: A case series, *World Neurosurg.* **83**, 657–663 (2015).
66. L. Ackermans, D. Annelien, C. van der Linden, M. Tijssen, K. Schruers, Y. Temel, M. Kleijer, P. Nederveen, R. Bruggeman, S. Tromp, V. van Kranen-Mastenbroek, H. Kingma, D. Cath, V. Visser-Vandewalle, Double-blind clinical trial of thalamic stimulation in patients with Tourette syndrome, *Brain* **134**, 832–44 (2011).
67. G. Schalk, D. J. D. J. McFarland, T. Hinterberger, N. Birbaumer, J. R. J. R. Wolpaw,

- BCI2000: A general-purpose brain-computer interface (BCI) system, *IEEE Trans. Biomed. Eng.* **51**, 1034–1043 (2004).
68. P. Stoica, R. L. Moses, *Spectral analysis of signals* (Pearson/Prentice Hall, 2005).
69. E. M. Rose, T. Mathew, D. A. Coss, B. Lohr, K. E. Omland, A new statistical method to test equivalence: an application in male and female eastern bluebird song, *Anim. Behav.* **145**, 77–85 (2018).
70. U. Meier, Nonparametric equivalence testing with respect to the median difference, *Pharm. Stat.* **9**, 142–150 (2009).
71. A. Sudhyadhom, M. S. Okun, K. D. Foote, M. Rahman, F. J. Bova, A Three-dimensional Deformable Brain Atlas for DBS Targeting. I. Methodology for Atlas Creation and Artifact Reduction, *Open Neuroimag. J.* **6**, 92–98 (2012).
72. T. A. Yousry, U. D. Schmid, H. Alkadhi, D. Schmidt, A. Peraud, A. Buettner, P. Winkler, Localization of the motor hand area to a knob on the precentral gyrus. A new landmark, *Brain* **120**, 141–157 (1997).
73. C. Cedzich, M. Taniguchi, S. Schafer, J. Schramm, Somatosensory evoked potential phase reversal and direct motor cortex stimulation during surgery in and around the central region., *Neurosurgery* **38**, 962–970 (1996).
74. S. A. Sheth, C. A. Eckhardt, B. P. Walcott, E. N. Eskandar, M. V. Simon, Factors affecting successful localization of the central sulcus using the somatosensory evoked potential phase reversal technique, *Neurosurgery* **72**, 828–834 (2013).
75. N. Maling, J. Shute, P. Rossi, C. de Hemptinne, J. Sanchez, B. Kretzman, A. Shukla, K. Foote, M. S. Okun, A. Gunduz, in (Neuroscience Annual Meeting 2014, Washington, DC, 2014).
76. N. J. Hill, D. Gupta, P. Brunner, A. Gunduz, M. A. Adamo, A. Ritaccio, G. Schalk, Recording Human Electrocorticographic (ECoG) Signals for Neuroscientific Research and Real-time Functional Cortical Mapping, *J. Vis. Exp.* (2012), doi:10.3791/3993.
77. B. B. Avants, N. J. Tustison, G. Song, P. A. Cook, A. Klein, J. C. Gee, A reproducible evaluation of ANTs similarity metric performance in brain image registration, *Neuroimage* **54**, 2033–2044 (2011).
78. B. B. Avants, C. Epstein, M. Grossman, J. Gee, Symmetric diffeomorphic image registration with cross-correlation: Evaluating automated labeling of elderly and neurodegenerative brain, *Med. Image Anal.* **12**, 26–41 (2008).
79. G. Schalk, E. C. Leuthardt, Brain-computer interfaces using electrocorticographic signals, *IEEE Rev. Biomed. Eng.* **4**, 140–154 (2011).
80. C. C. Aggarwal, *Data classification : algorithms and applications* (Chapman and Hall, New York, ed. 1st, 2014).

Acknowledgments: We thank the patients for their availability and help in this study. We also want to thank K. Rizer for his administrative support. **Funding:** This work was supported by the NIH BRAIN Initiative through NINDS grant UH3NS095553 to A.G., K.D.F.

Author contributions: Conceptualization, E.O., T.D., A.G., K.D.F.; Data curation: E.O.,

L.A., R.E.; Formal analysis: E.O.; Funding Acquisition: A.G., K.D.F.; Investigation, E.O., S.C., R.M., K.D.F.; Methodology: E.O.; Project administration: E.O., A.G.; Resources: A.G., T.D., M.S.O., K.D.F.; Software: E.O.; Supervision: A.G., M.S.O.; Visualization: E.O., R.E., J.C.; Writing – Original Draft, E.O., A.G.; Writing – Review & Editing, A.G., S.C., T.D., M.S.O., K.D.F. **Competing interests:** Dr Almeida has provided educational consulting and participated in advisory boards, therefore receiving honoraria for such activities, for Medtronic and Boston Scientific. Dr. Denison is a paid consultant for Synchron, Cortec Neurotechnology, and Inspire Sleep Therapy. His research is funded by the MRC (UK), DARPA, the Royal Academy of Engineering, and multiple foundation sources. Implantable devices for Dr. Denison's DBS-related research have been provided by Medtronic and Bioinduction. (Medtronic has provided implantable devices and some technical support for the current study). He was a VP of Research and Technology at Medtronic through August 2018. He has multiple patents in the area of brain-machine-interfacing and DBS (9,248,288 and 8,380,314: patient directed therapy control; 8,554,325: therapy control based on a patient movement state), all licensed to Medtronic, but receives no royalty payments. Dr. Okun serves as a consultant for the Parkinson's Foundation, and has received research grants from NIH, Parkinson's Foundation, the Michael J. Fox Foundation, the Parkinson Alliance, Smallwood Foundation, the Bachmann-Strauss Foundation, the Tourette Syndrome Association, and the UF Foundation. Dr. Okun's DBS research is supported by: R01 NR014852 and R01NS096008. Dr. Okun has received royalties for publications with Demos, Manson, Amazon, Smashwords, Books4Patients, Perseus, Robert Rose, Oxford and Cambridge (movement disorders books). Dr. Okun is an associate editor for New England Journal of Medicine Journal Watch Neurology. Dr. Okun has participated in CME and educational activities on movement disorders sponsored by the Academy for Healthcare Learning, PeerView, Prime, QuantiaMD, WebMD/Medscape, Medicus, MedNet, Einstein, MedNet, Henry Stewart, American Academy of Neurology, Movement Disorders Society and by Vanderbilt University. The institution and not Dr. Okun receives grants from Medtronic, Abbvie, Abbott and Allergan and the PI has no financial interest in these grants. Dr. Okun has participated as a site PI and/or co-I for several NIH, foundation, and industry sponsored trials over the years but has not received honoraria. Research projects at the University of Florida receive device and drug donations. Dr. Foote has received occasional consulting fees from Medtronic and Boston Scientific. His research is primarily funded by NIH and multiple foundation sources. Implantable devices for Dr. Foote's DBS-related research have been provided by Medtronic and Neuropace. (Medtronic has provided implantable devices and some technical support for the current study.) Dr. Foote has participated as a site implanting surgeon in multicenter DBS-related research studies sponsored by Abbott/St. Jude, Boston Scientific, and Functional Neuromodulation. The University of Florida receives partial funding for Dr. Foote's functional neurosurgery fellowship from Medtronic. **Data and materials availability:** All data associated with this study are available in the main text or the Supplementary Materials.

Figures:

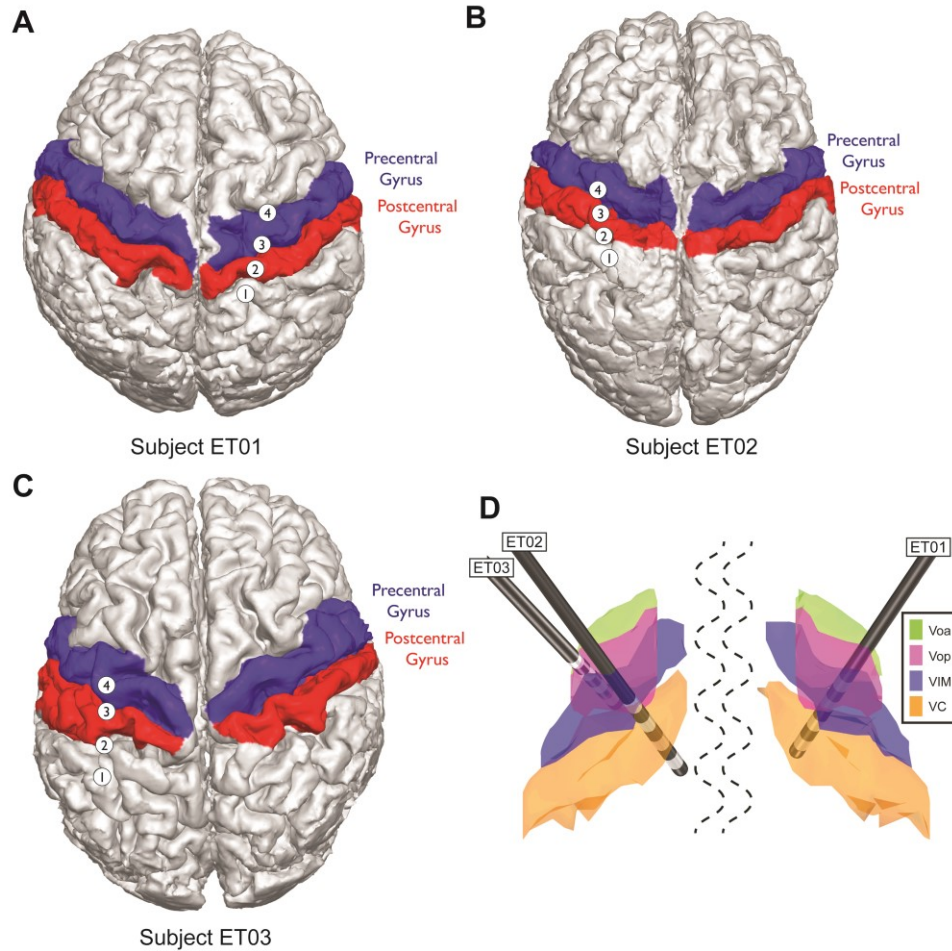


Fig. 1. Patient specific MRI-CT reconstruction and segmentation of cortical and thalamic regions in ET CL patients. (A) Subject ET01, (B) Subject ET02, (C) Subject ET03 cortical segmentations. In red is the postcentral gyrus, in blue the precentral gyrus, known as primary motor cortex (M1). (D) Subcortical thalamic segmentation with overlaid the DBS lead positioning based on surgical planning and all normalized to an MNI brain. The structures shown are: ventralis oralis anterior (green, Voa), ventralis oralis posterior (magenta, Vop), ventralis intermediate nucleus (blue, VIM), nucleus ventralis caudalis (orange, VC).

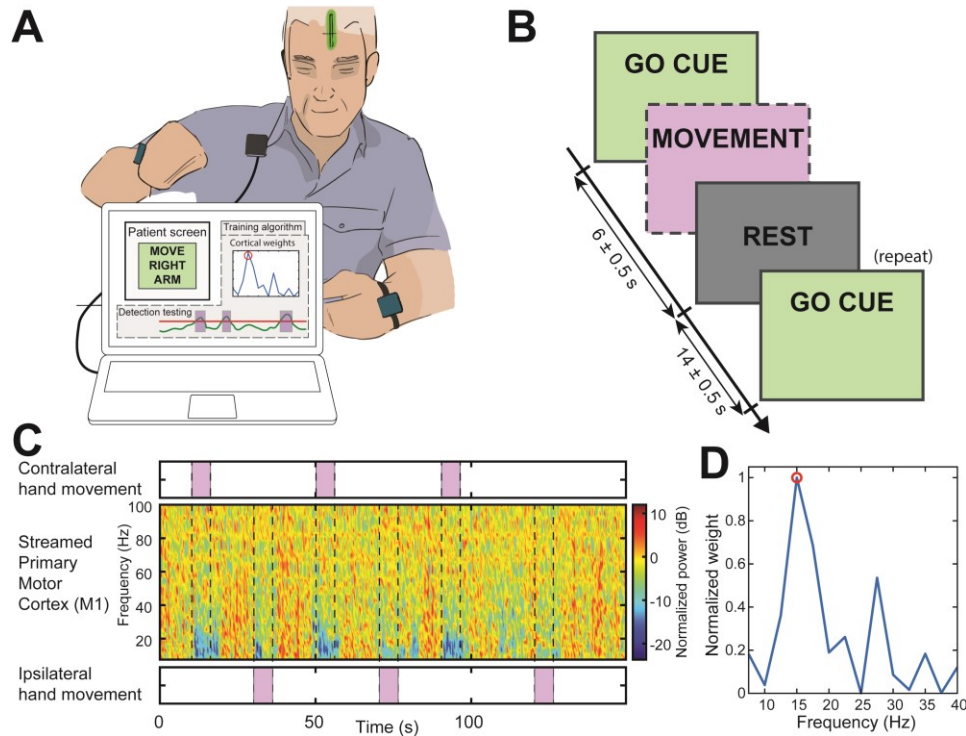


Fig. 2. Training session for onboard movement detection. (A) Setup for the training of the onboard weights used by the embedded LDA to actuate the stimulation. The patient is prompted to move (visual GO CUE) while data are being streamed through Nexus-D telemetry wand from the cortical strip (shown as a green strip in the patient head) to an external computer (the training algorithm output is not shown to the patient). (B) Task timeline of the recordings. The boxes with a dashed border indicate the un-cued actions the subject took during the task. The patient was cued (GO CUE) to execute arm movement (with left or right arm) until the REST cue was delivered. The task was repeated interleaving the hands used in a randomized pattern. (C) Spectrogram collected from M1 through the telemetry wand, aligned with the executed cued movement (contralateral and ipsilateral). The spectrogram was used as features for a Fisher score feature selection algorithm, for which the output is shown in (D). One or two features were selected and the Activa PC+S neurostimulator was setup accordingly. After identifying the features of interest, the same paradigm was repeated to obtain the weights and threshold for the stimulation delivery based on power features.

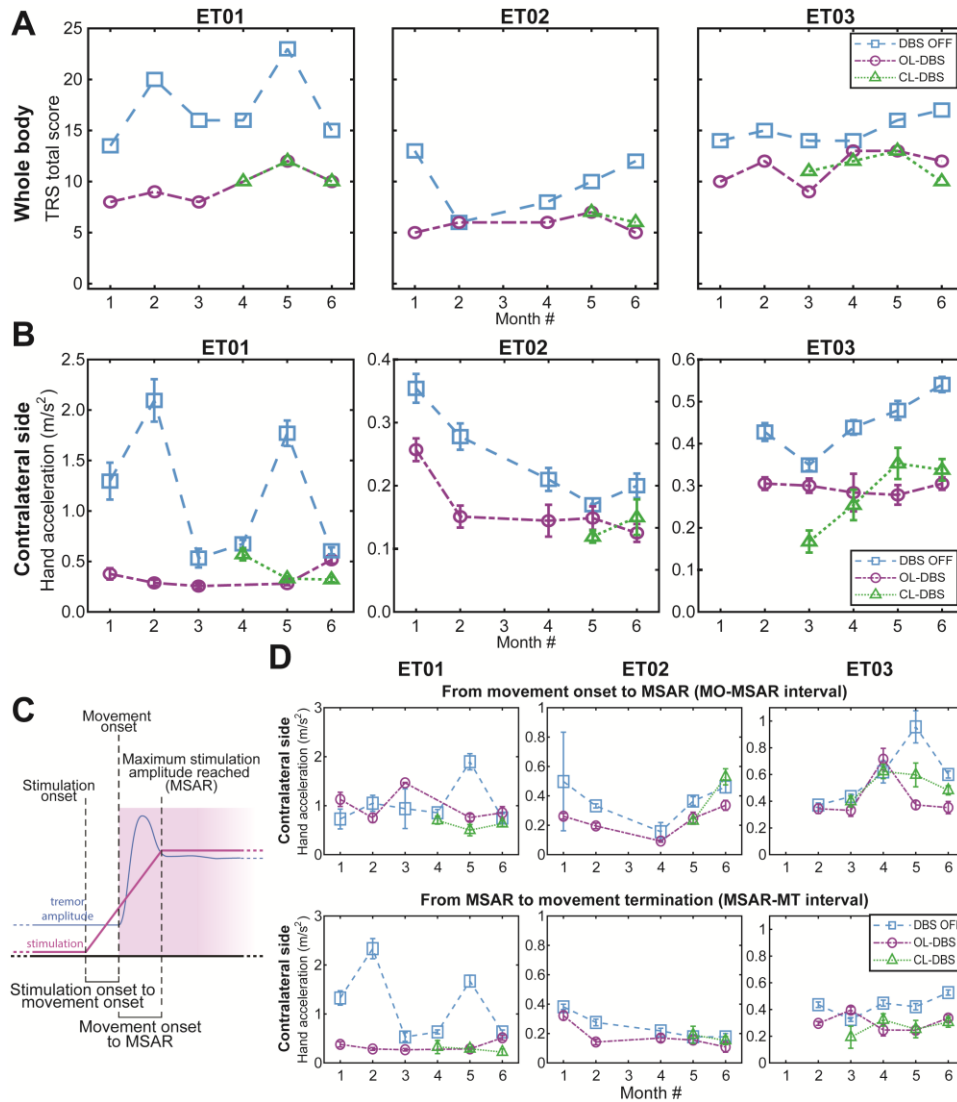


Fig. 4. Longitudinal clinical outcomes for closed-loop DBS during specific stimulation and movement events. (A) Clinical Tremor Rating Scores (TRS) over 6 months visits across different DBS modalities. Closed-loop DBS scores are presented starting with the month it was established in each patient. For patient ET01 the score for OL-DBS is missing on month 4 due to subject exhaustion. For patient ET02 month 3 scores were not assessed due to medical reasons unrelated to the study. (B) Tremor amplitude based on acceleration during the execution of the TRS clinical assessment shown in (A). For patient ET03 month 1 inertial data during TRS evaluation was not collected. (C) Diagram of the subdivisions of interest: stimulation onset (SO), movement onset (MO), time maximum stimulation amplitude reached (MSAR), movement termination (MT), delay movement onset to stimulation onset (interval MO-SO), delay movement onset to MSAR (interval MO-MSAR). (D) Tremor amplitude based on acceleration during the execution of the TRS clinical assessment over 6 monthly visits across different DBS modalities, as shown in (A-B). (D top) is the tremor amplitude during the MO-SO interval whereas (D bottom) is the tremor amplitude during MSAR-MT interval). For patient ET01 the score for OL-DBS is missing on month 4 due to subject exhaustion. For patient ET02 month 3

scores were not assessed due to medical reasons unrelated to the study. For patient ET03 month, inertial data during TRS evaluation was not collected. DBS OFF and OL-DBS settings do not have a ramp-up interval and to achieve a comparison across different DBS settings (DBS OFF, OL-DBS, CL-DBS), we use the MO-MSAR interval from the CL-DBS recorded during the same month. If no CL-DBS was executed during that month, we used the patient-matched MO-MSAR average.

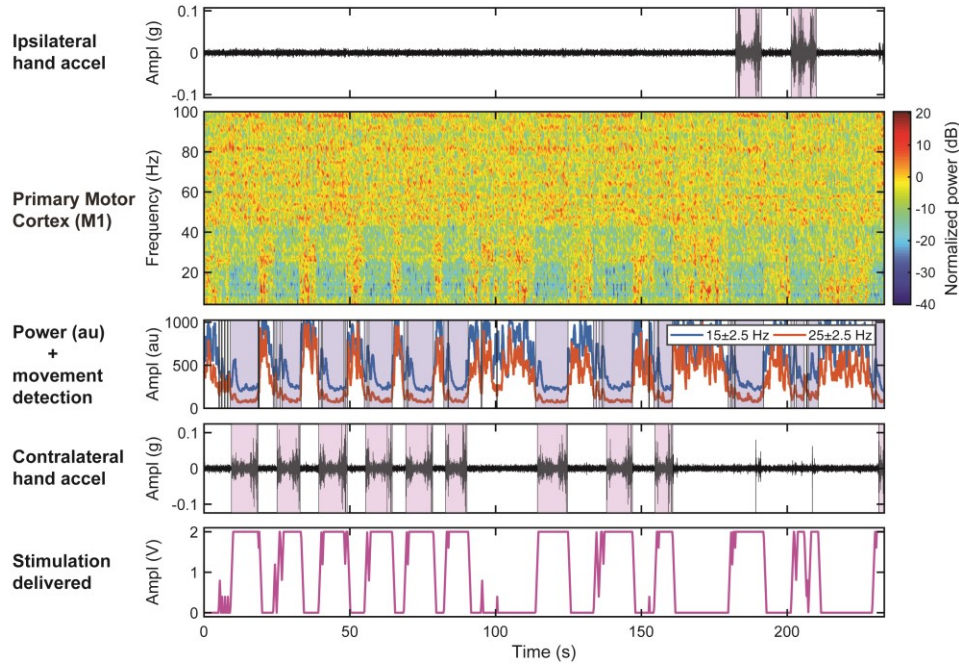


Fig. 5. Implementation of closed-loop DBS in patient affected by ET (ET01, 3rd month).

Brain activity was recorded during a volitional reaching task with simulated drinking (patients reached for the cup, brought it close to their mouths and put it back) along with ipsilateral and contralateral hand accelerometer traces. The violet boxes represent the movement initiation towards the target (cup). The second row shows the normalized spectrogram of the right primary motor cortex collected chronically from a patient affected by ET and implanted with Activa PC+S. Two power bands centered at 15Hz and 25Hz with 5Hz bandwidth obtained with Fisher score feature selection were used as inputs to the linear discriminant analysis classifier embedded event detector (blue blocks indicate movement detection). The bottom row shows the output of the embedded event detector triggered closed-loop stimulation (stim range=0-2V, ramp-up/down=2V/s, frequency=130 Hz, pulse width 120 μ s).

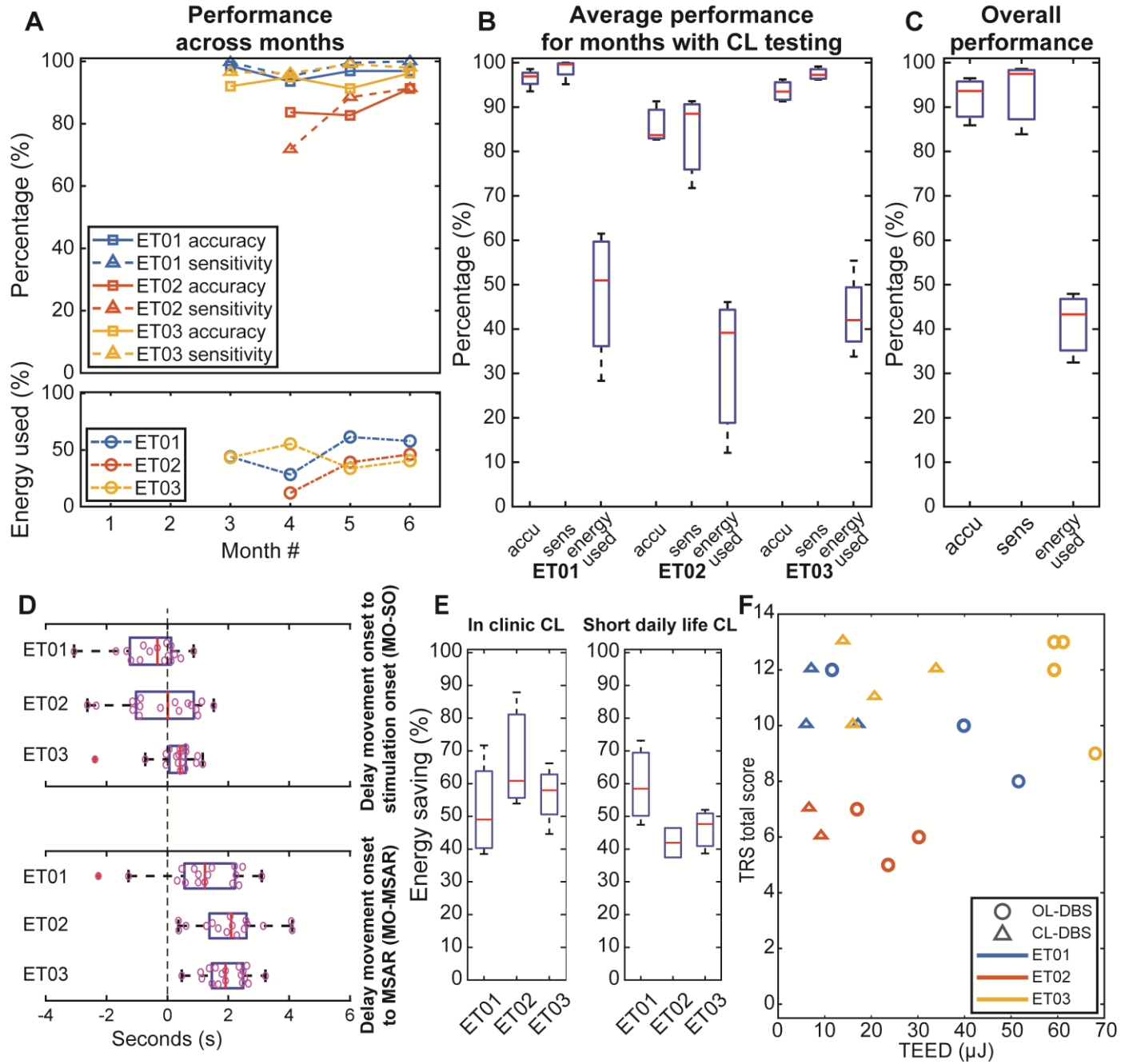


Fig. 6. Performances of closed-loop DBS at monthly visits in all the enrolled subjects using the fully embedded onboard PC+S algorithm. (A) Performances over the monthly clinical/research-visit, such as accuracy and sensitivity of the CL-DBS classifier on top, and energy usage compared to energy usage (TEED) of continuous stimulation (with CL-DBS settings delivered as open-loop paradigm) at the bottom. (B) Average performances across months with closed-loop DBS during clinical/research visit. (C) Average performances of closed-loop DBS, including energy usage compared to energy usage (TEED) of continuous stimulation (with CL-DBS settings delivered as open-loop paradigm). (D) Characterization of the delays in the CL-DBS implementation (intervals MO-SO, MO-MSAR). (E) Energy saving with closed-loop stimulation compared to

continuous stimulation (with CL-DBS settings delivered as open-loop paradigm), respectively during clinical/research-visit (as in A bottom, B, and C) and at short-term daily life usage. (F) TRS vs total electrical energy delivered (TEED) scatterplot, showing a subject based decrease in the overall CL-DBS TEED compared to OL-DBS, while maintaining a comparable TRS. TEEDs are normalized to the duration of the task, to avoid bias due to each task length.

Supplementary Materials:

Materials and Methods

Selection criteria

Subjects were enrolled in our study if they qualified within the inclusion and exclusion criteria as reported at Clinicaltrials.gov: NCT02649166. No patients were excluded after implantation of the Activa PC+S.

Here we summarize the inclusion criteria: subject diagnosed with a postural-intention (essential) tremor for at least 3 years; subject had a notable disabling medical-refractory upper extremity tremor with no evidence of supraspinal central nervous system disease or injury (tremor not adequately controlled by medications for at least three (3) months before implant); subject had a postural or kinetic tremor severity score of at least 2 out of 4 in the extremity intended for treatment on the Fahn-Tolosa-Marin Clinical Rating Scale for Tremor (TRS); subject had a TRS score of 2 or above in any one of the items 16-23 from the Disability subsection of the TRS: speaking, feeding other than liquids, bringing liquids to mouth, hygiene, dressing, writing, working and social activities; subject tremor is refractory adequate trials of at least two medications, one of which should be either propranolol or primidone. An adequate medication trial is defined as a therapeutic dose of each medication or the development of side effects as the medication dose is titrated.

Here we summarize the exclusion criteria: subject had previous neurosurgical intervention including deep brain stimulation or ablative brain lesions; presence of any other medication related movement disorders; suspicion of Parkinsonian tremor, including presence of Parkinsonian features such as bradykinesia, rigidity, or postural instability; subject presents behaviors consistent with ethanol or substance abuse as defined by the criteria outlined in DSM-V; severe medical co-morbidity including cardiovascular disorder, lung disorder, kidney disease, continuous neurological disease, hematological disease, or frailty that impact tolerability of the surgery as judged by the screening physicians; abnormal brain MRI including hydrocephalus, stroke, structural lesions, demyelinating lesions, or infectious lesions. Also excluded are subjects with severe atrophy; any uncontrolled symptoms or signs of increased intracranial pressure (such as headache, nausea, vomiting, lethargy, papilledema); history of seizures within the past year; dementia rating scale score (DRS) <130 signifying notable cognitive dysfunction and a potential for inability to cooperate with tasks involved in the study; attempt or intent of suicide in the last six month; presence or history of psychosis; notable or active mood disorders including depression; ongoing pregnancy or planning near-future pregnancy.

Surgical Procedure

The electrode implant configuration consisted of 2 leads (total of 8 contacts, 4 contacts for each lead): lead 1, Medtronic model 3387 DBS lead placed in ventralis intermediate nucleus (VIM); lead 2, Medtronic Resume II (model 3587A) ECoG subdural strip over primary motor (M1) cortices. These leads were implanted contralateral to the side with worse tremor. To localize the VIM target, T1 structural MRIs were fused to a stereotactic head CT and co-registered to a UF-developed 3D deformable brain atlas, that was adapted to match the patient brain in order to predict the location of the VIM region as accurately as possible (71). After a safe trajectory to the selected target was chosen, a burr hole was drilled in the skull at the trajectory entry site. Anesthetic was delivered locally at the site of the implantation, allowing the patient to stay

awake during the surgery. A microelectrode was advanced through the brain along the planned trajectory using a micropositioner to allow for intermittent single unit recording with an FHC 4000 LP+ system (FHC) and to precisely identify the VIM/Nucleus Ventralis Caudalis (VC) boundary. Before the initiation of any recordings or functional mapping, the patient sedatives were stopped. A neurologist evaluated the neural firing in response to stimuli/commands (touch, volitional movements, light cues) to verify if the brain region activity matched the expected firing patterns. When the target was localized, the microelectrode was substituted with the DBS macroelectrode. Target location was tested through intraoperative macrostimulation for effectiveness of tremor suppression and stimulation induced side effects (such as paresthesia and capsular pulling). The cortical strip was inserted through the same burr hole made for the VIM lead in an effort to avoid increasing the complexity of the surgery. The subdural ECoG strip was placed proximal to the hand knob (72), over the PM, M1 and primary somatosensory (S1) areas which were estimated from the fused MRI-CT reconstruction. PM and M1 areas were localized through somatosensory evoked potentials (SEP)(73, 74) and real-time functional mapping of hand function (75). For the latter, the implanted cortical strip was connected to an external FDA approved bioamplifier (g.HiAmp, Guger Tech) and a modified SIGFRIED protocol were executed (76). The protocol required the creation of a baseline model of high gamma activity at rest/baseline, subsequently testing for different conditions/commands (task block=10s, interstimulus intervals [ISI]=10s). The conditions tested were “open and close left hand”, “open and close right hand”, “kiss” (puckering lips) and these were repeated until the stop cue was presented. The algorithm outputted the likelihood of the activity from each electrode to be associated with a specific task, dependent on the high gamma divergence from the baseline model in each block. The “kiss” condition was inserted as a control condition, to verify that the ECoG strip was not over the face motor area. Once the placement was verified, an intraoperative CT was executed and, together with preop-MRI, was used to generate brain models to localize the electrode positions for each patient. At the end of the recording, the patient was sedated, and the leads were chronically connected to the Activa PC+S. The cortical strip was left in place as required by the study design and as approved by FDA.

Imaging

MRI-CT fusion was achieved with the use of ANTs toolbox (77, 78) to enable the visualization of electrode contacts together with patient anatomy. Cortical reconstructions and segmentations were performed using the Freesurfer image toolbox, which enabled the visualization of the electrodes with respect to the segmented anatomy and to verify the correct placement of the cortical strip in relation to M1. For the subcortical structures, an adapted digitized Schaltenbrand-Bailey atlas was manually fitted to each patient’s structural imaging, using a linear affine transformation without shearing (71). This modality was the same used during the surgical planning for the targeting of the DBS electrode.

Movement Events

Movement events within each block were marked via visual inspection of accelerometer traces, EMG and video data, obtaining 6 total event types: baseline, baseline epochs within the task (inter-movement intervals), cue for right hand movement, cue for left hand movement, right hand movement, and left hand movement. The same subdivision was used for both cued hand opening and closing, and cued cup reaching.

Training session for onboard movement detection with a computer-in-the-loop

To achieve an efficient programming of the embedded linear discriminant analysis (LDA) classifier, a test bench algorithm was built using the Medtronic telemetry wand, which facilitated interfacing with the neurostimulator to stream data in real time to a computer with a configuration and noise which was the most similar to the embedded use-case. Viable neuromarkers were limited to be between the 5.5 to 37.5 Hz due to device noise limitations with poor signal to noise ratio (SNR) at higher frequencies. Nonetheless, this lets us detect movement considering how low frequency oscillations (LFOs) modulated for both contralateral and ipsilateral movement (79), with prominent alpha-beta decrease during contralateral movement.

The training session consisted in a short sequence of interleaved cued arm movements (task timeline in Fig. 2B), while real-time streaming the data through the Medtronic telemetry wand placed over the implant (setup shown in Fig. 2A, data collected during a single session shown in Fig. 2C). A maximum of 2 power bands were available for the cortical contact (3 with bridging-mode, which can introduce additional distortions). After an initial screening for the most salient features to use for the closed-loop algorithm using Fisher score feature selection (80), we selected preferably only one power band (Fig. 2D) and configured it on the onboard PC+S power estimator. Two power bands were included when two substantially different (in frequency) but comparable (in magnitude) peaks were found in the weight values (such as the 15 and 25 Hz case) during the feature selection step. In some cases (ET02) two power bands were chosen to better mitigate misclassification due to stimulation artifacts, as stimulation artifact may cause an increase of the overall power estimate through a leakage in the hardware-based power estimators embedded in the Aactiva PC+S (Fig. S9). Hence, we proceeded to re-execute the training task to estimate the correct thresholds for embedded movement detection. Noting how LFO activity decreased for both contralateral and ipsilateral movement, we aimed to achieve tremor suppression for both movements. However, the classifier performances were concentrated on the delivery of stimulation during the contralateral limb movement, which is the most affected by tremor and the target of this therapeutic implementation. Considering that stimulation could possibly be beneficial during either limb movement, with a largely pronounced benefit to the upper limbs contralateral to the stimulation target, this was considered an appropriate stimulation policy. The weights obtained were tested briefly in real time with the usage of a tablet dedicated to interfacing with the sensing capabilities of the PC+S device. Once fully programmed, the testing proceeded to check performances of the closed-loop with cued and volitional cup reaching tasks.

Classification performance and energy consumption

The total electrical energy delivered (TEED) was computed based on the method described by Koss et al. (38), expanded to the closed-loop case, as in our case the voltage changes over time. TEED is normalized with respect to the time of the task.

$$TEED_{1sec} = \frac{\int_T V(t)^2 dt \cdot freq \cdot pw}{R} \cdot \frac{1}{T} \cdot (1 sec)$$

Where $V(t)$ is the instantaneous voltage delivered by the neurostimulator, T is the total time of the run in consideration, $freq$ is the constant stimulation frequency, pw is the constant stimulation pulse width, R is the impedance between the stimulation contacts. Hence, $TEED_{1sec}$ is the average TEED in 1 sec of time.

The classifier performances, such as accuracy, sensitivity and precision, were computed based on the stimulation estimate trace, obtained combining the stimulation amplitude ramp-up and ramp-down information to the onboard detection state trace. The performances are referred to the detection of the contralateral limb, which is the tremor affected limb needing the most suppression through DBS delivery. The minimum amplitude (in V) necessary to be considered as stimulation delivered (DBS ON) state was set at 0.5V. The choice of using the stimulation estimate trace was made because DBS was delivered based on the set increase and decrease rates (voltage ramp-up and ramp-down), which act as a de-facto low pass filter, smoothing the detection profile, and not just on the detection onset/termination (Fig. S10). The stimulation estimate trace was used as one of the inputs, $V(t)$, for the TEED estimation. It should be pointed out that these energy savings do not reflect the energy required for sensing capabilities of the device, which is minor compared to stimulation demands (28, 29, 39). Khanna et al. reported that CL-DBS would have to be triggered 94% of the time for it to have equal energy use as open-loop paradigm using the same DBS parameters (frequency, amplitude, pulse-width) (26).

Supplementary Figures

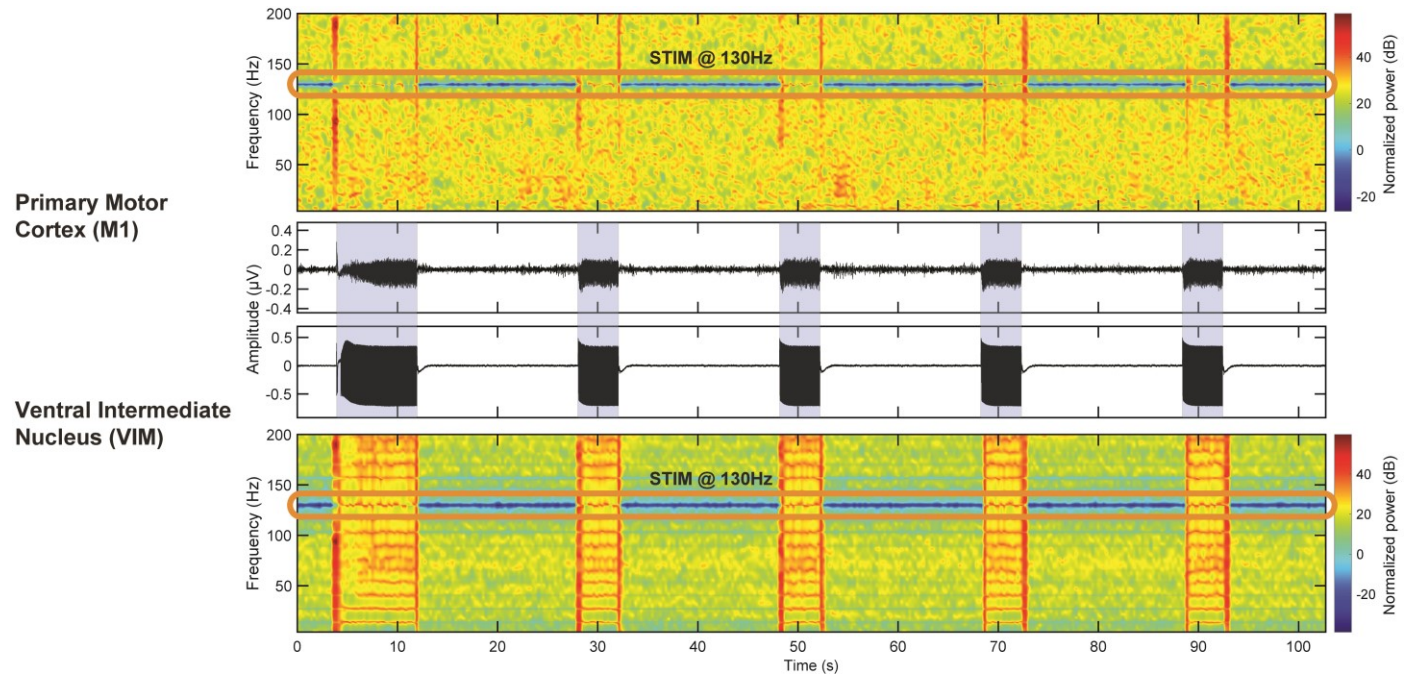


Fig. S1.

Artifacts from stimulation impaired data collection from VIM contacts. The artifacts presence is due to DBS-induced saturation of the recording channels connected to contacts adjacent the stimulation contacts. This is clearly visible in both the raw trace and spectral estimate. Data were collected with the subject at rest while delivering stimulation in small intervals. Blue blocks represent when stimulation was being delivered. Stimulation parameters were 130 Hz, 2.0 V, pulse width at 120 μs .

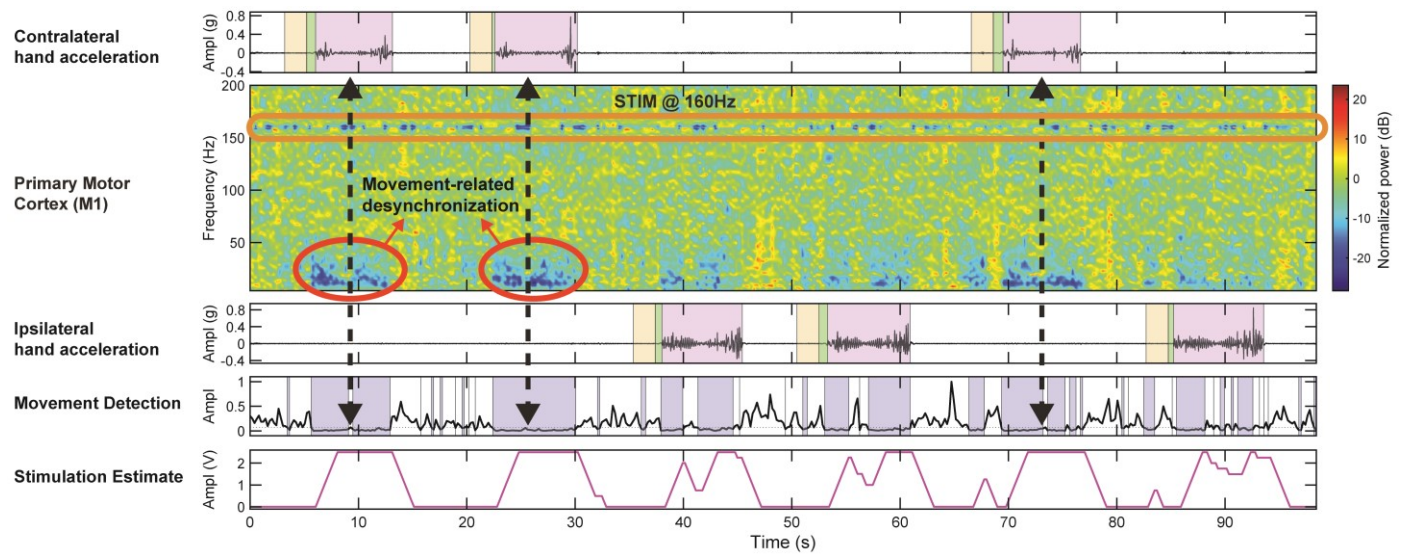


Fig. S2.

Artifacts from stimulation did not impair movement detection performances from cortical contacts. Data collected during a single cued-go cup reaching task along with contralateral and ipsilateral hand accelerations, with respect to the side of implantation. Data were recorded purely from the chronic Activa PC+S, while delivering OL-DBS at 160Hz at 3.0V (pulse width at 90 μ s) (circled in orange), along with contralateral (top) and ipsilateral (bottom) hand accelerations. The subject was asked to prepare to move with the CUED hand (yellow). The GO CUE event (green) represents when the subject was asked to reach the cup, and the MOVEMENT event (violet) represents when the patient proceeded to execute the movement. The bottom plots show the algorithm used for simulating the embedded movement detection (blue block when there is a movement detection), and predicting the stimulation profile (stimulation estimate). The features used in the stimulation prediction were trained from a cued cup task without stimulation. The features were still visible even with stimulation artifact (circled in red). The device was in OL-DBS mode.

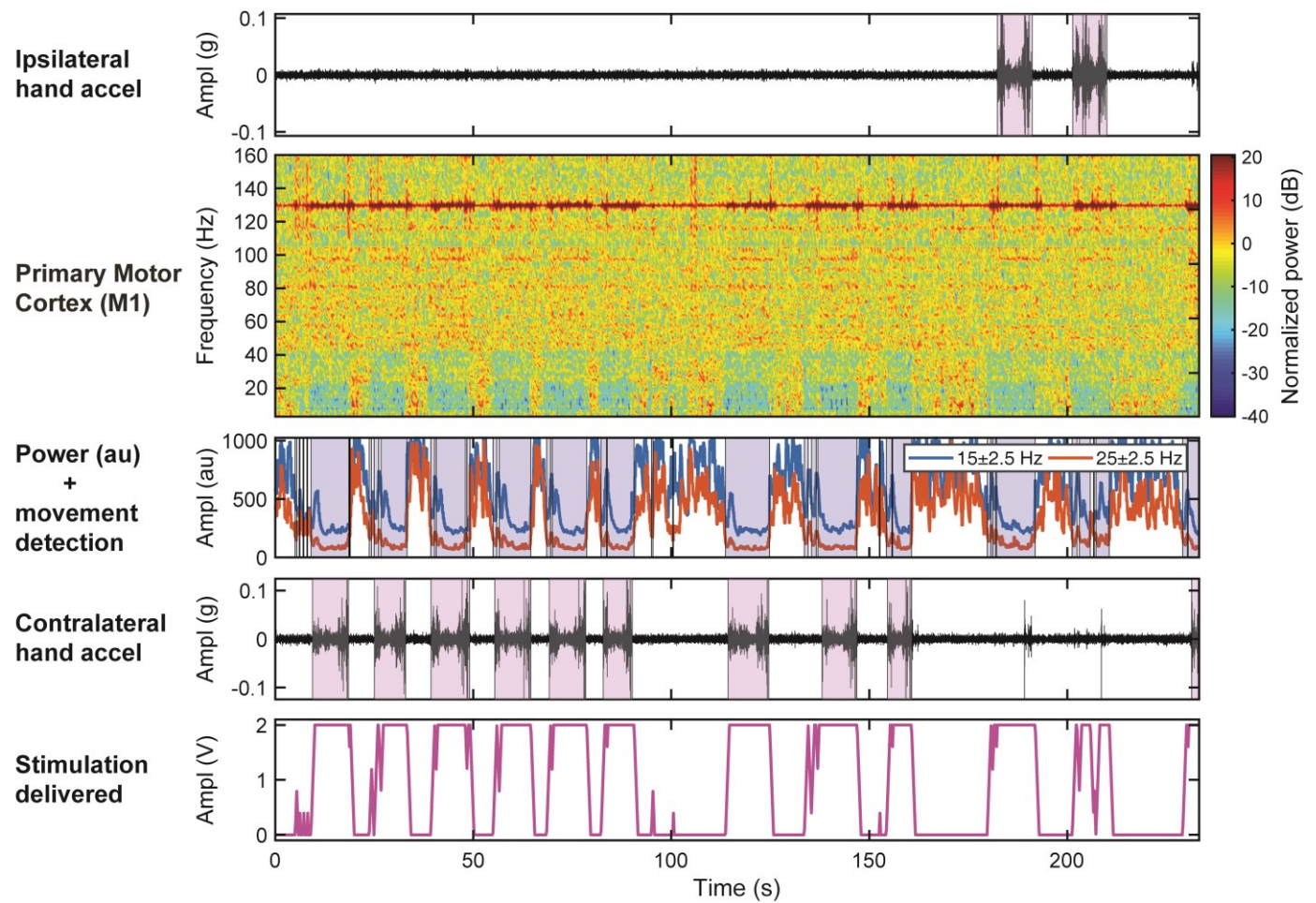


Fig. S3.

Implementation of closed-loop DBS in a patient affected by ET showing spectral leakage of the stimulation artifact. Same trial shown in Fig. 5 with a wider frequency for the spectral analysis. Brain activity was recorded during a volitional reaching task with simulated drinking (patients reached for the cup, brought it close to their mouths and put it back) along with ipsilateral and contralateral hand accelerometer traces. The violet boxes represent the movement initiation towards the target (cup). The second row shows the normalized spectrogram of right primary motor cortex collected chronically from a patient affected by ET and implanted with Activa PC+S. Two power bands centered at 15Hz and 25Hz with 5Hz bandwidth obtained with Fisher score feature selection were used as inputs to the linear discriminant analysis classifier embedded event detector (blue blocks indicate movement detection). The bottom row shows the output of the embedded event detector triggered closed-loop stimulation (stim range=0-2V, ramp-up/down=2V/s, frequency=130 Hz, pulse width 120 μ s).

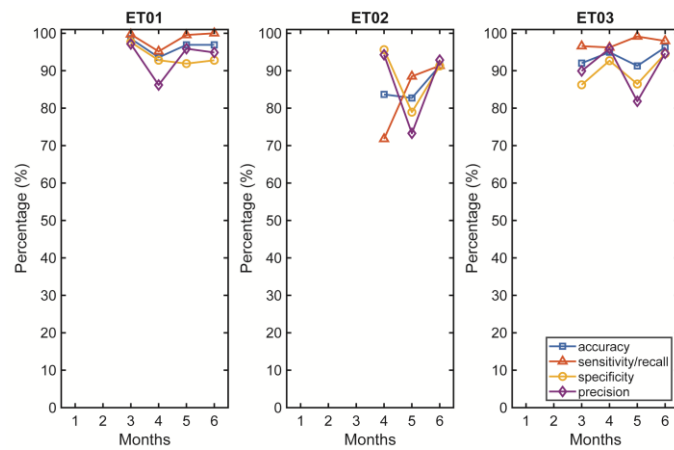


Fig. S4.

Performances of the embedded detector over the monthly clinical/research visit in all the enrolled subjects. This figure further details the embedded detector performances shown in Figure 6A top, adding further classifier outcomes measures (specificity, precision). The CL-DBS algorithm was fully embedded in the PC+S.

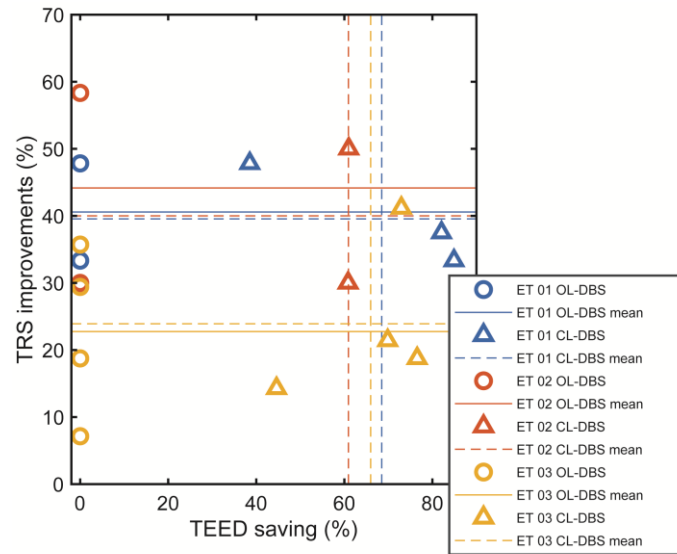


Fig. S5.

TRS improvements vs TEED savings in percent. The scatterplot shows showing a subject-based decrease in the overall TEED, while maintaining a comparable TRS. TRS improvements (percent) are expressed with respect to TRS scores with DBS OFF. TEED savings percent are expressed with respect to TEED during OL-DBS. TEEDs (in OL-DBS and CL-DBS) were indicated as TEED per second, to avoid bias due to each task length.

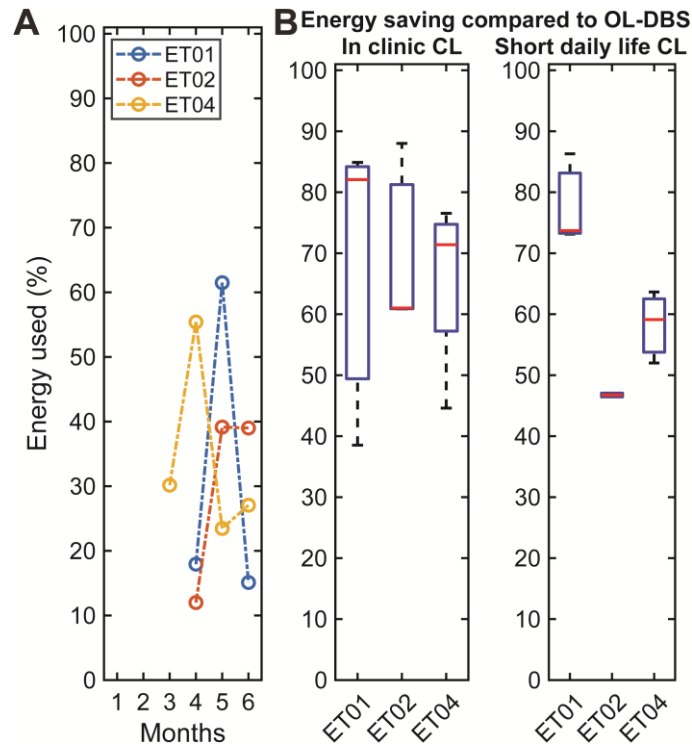


Fig. S6.

Energy performance of closed-loop DBS at monthly visits in all the enrolled subjects compared to open-loop DBS energy consumption (TEED). (A) Energy savings compared to open-loop stimulation TEED over the monthly clinical/research visit. (B) Energy saving with closed-loop stimulation (compared to open-loop stimulation TEED), respectively in clinic and at short-term daily life usage. Short-term daily usage refers to CL-DBS tested between two consecutive daily visits, from the afternoon to the morning of the next day, during a typical daily real-life usage.

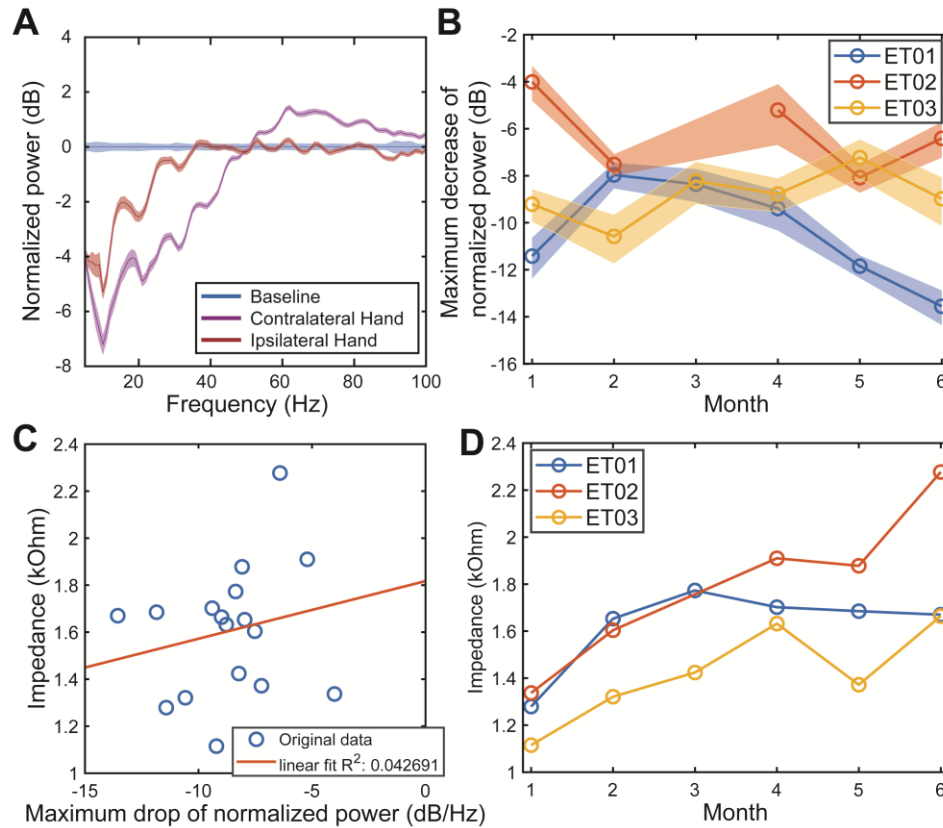


Fig. S7.

PSD and impedance over 6 months period. (A) Group average of normalized PSD profiles for contralateral (red) and ipsilateral (violet) movement tasks. (B) Maximum PSD drop in the low frequency oscillation (LFO) band in M1 during contralateral movement execution normalized to baseline across all patients. (C) Group analysis of maximum LFO PSD drop from M1 during contralateral movement and impedance across the same contacts used for recording the signal from M1 showed no correlation. (D) Impedance of bipolar contacts combinations used for recording the M1 region at each monthly visit across all patients.

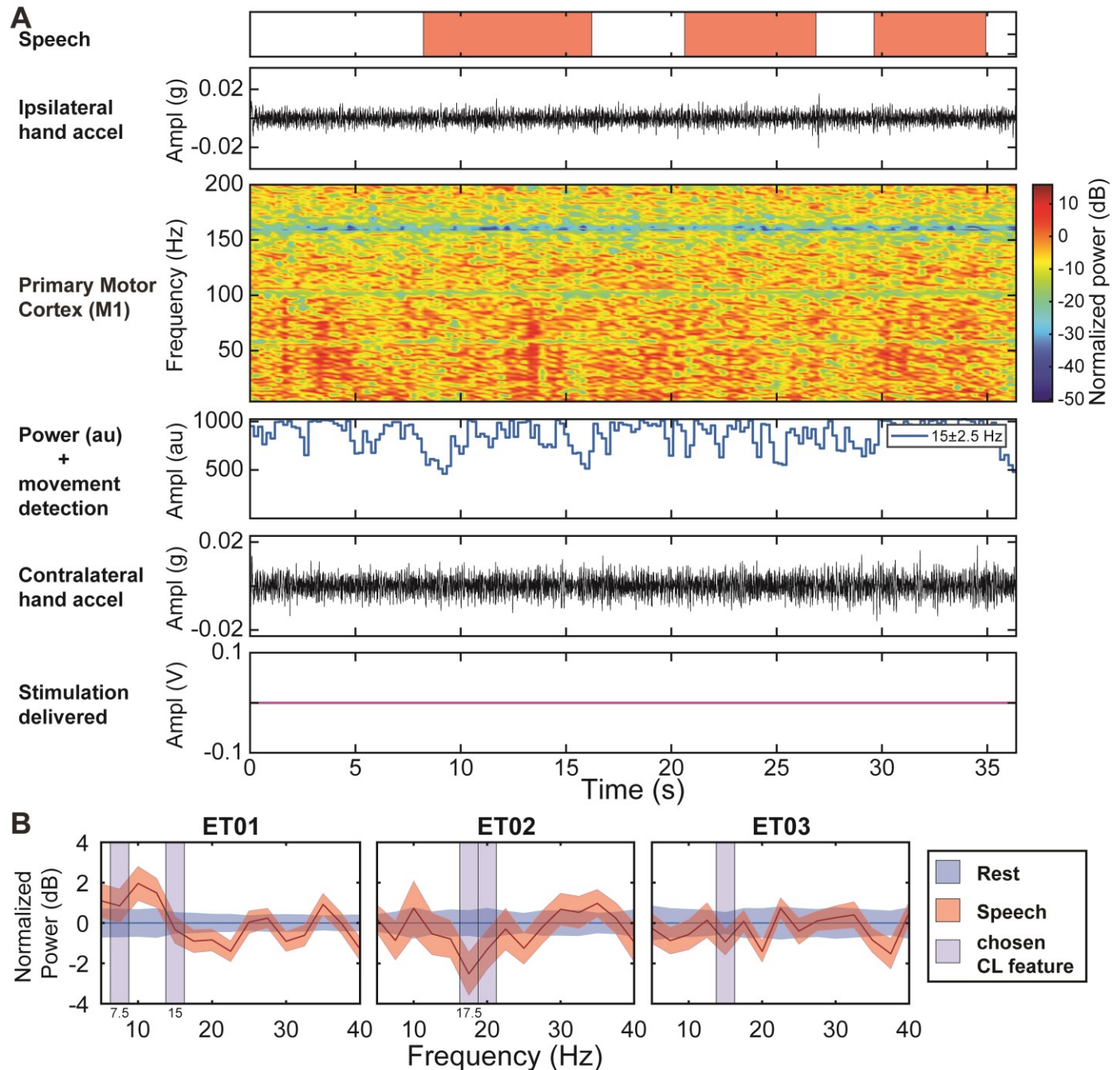


Fig. S8.

Performance of closed-loop DBS in patients affected by ET during speech execution. In the upper area (A) a single patient recording is shown (ET03, 5th month). Brain activity was recorded during along with voice state (speech as red, absent if not) ipsilateral and contralateral hand accelerometer traces. The violet boxes represent the movement initiation towards the target (cup). The third row shows the normalized spectrogram of right primary motor cortex collected chronically from a patient affected by ET and implanted with Acliva PC+S. One power band centered at 15Hz with 5Hz bandwidth obtained with Fisher score feature selection was used as inputs to the linear discriminant analysis classifier embedded event detector (blue blocks indicate

movement detection). The bottom row of (A) shows the output of the embedded event detector triggered closed-loop stimulation (stim range=0.0-2.5V, ramp-up=2.5V/s, ramp-down=0.83V/s, frequency=160 Hz, pulse width 90 μ s). As expected, the embedded detector did not detect speech execution (sensitivity=0%, specificity=100%). The reported detection measures are referred to the detection of speech execution, and not of movement. (B) Normalized PSD profiles of the same speech execution task shown in (A) executed in all 3 ET patients. The deviation of power during speech, compared to rest, in the chosen CL feature bands (ET01 feature 7.5Hz: 0.8463 dB [SE=0.1369 dB, t_{86} = 1.4342, P =0.1551], feature 15Hz: -0.3337 dB [SE=0.1103 dB, t_{86} = 0.3130, P =0.7551]; ET02 feature 17.5Hz: -2.5164 dB [SE=0.2144 dB, t_{74} =-0.4671, P =0.6418], feature 20Hz: -1.3099 dB [SE=0.1972 dB, t_{74} =-1.4132, P =0.1618]; ET03 feature 15Hz: -0.9320 dB [SE=0.1106, t_{60} =0.02405, P =0.9809]) was not sufficient to elicit the delivery of full therapeutic stimulation.

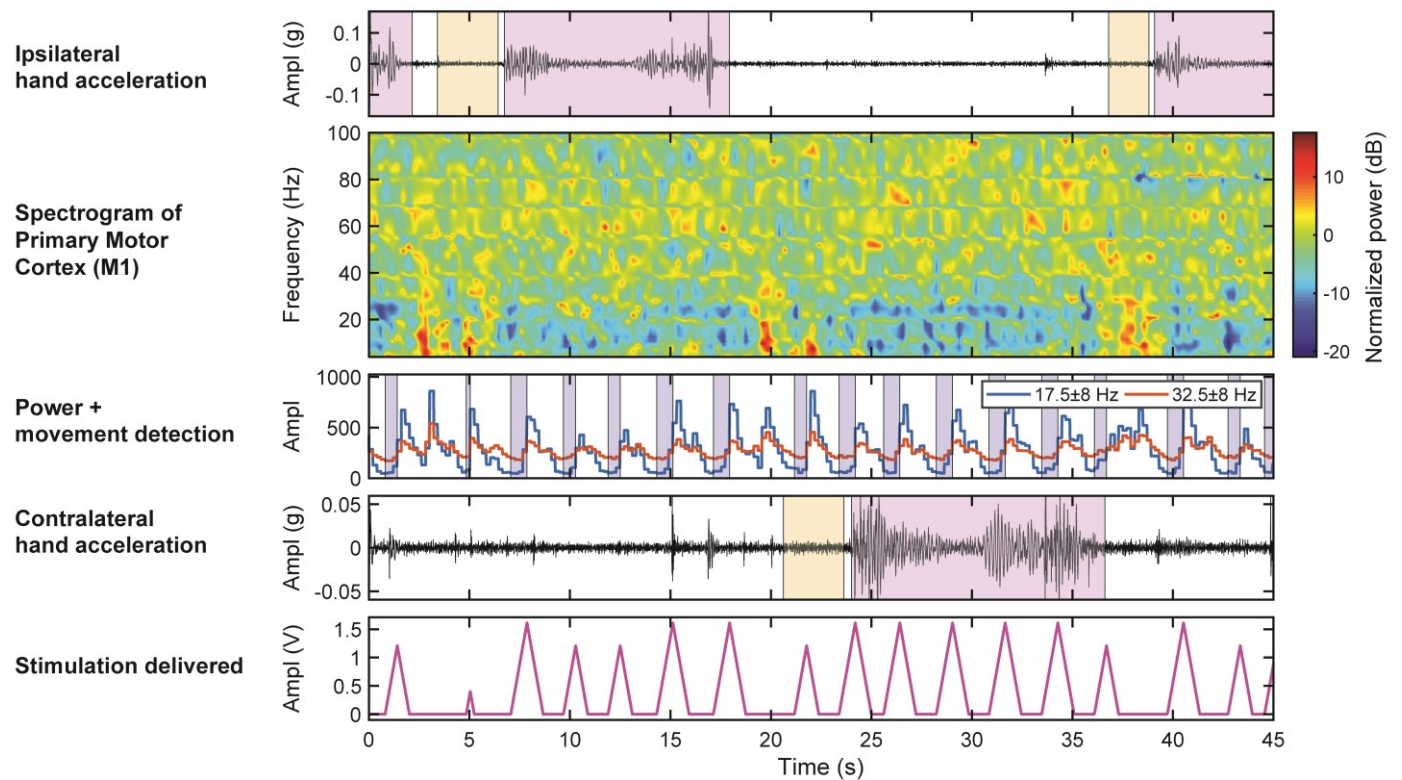


Fig. S9.

Example of a non-optimized embedded closed-loop stimulation paradigm. The power channels are computed by analog power estimators, which differ from the ADC sampling the time domain signal. Hence, the power estimates can be affected by artifacts and configurations not observed in the time domain. In this run, the stimulation amplitude increase affected the movement-related low frequency oscillations estimates, causing a continuous toggling between detected and undetected status. Further adjustments to the stimulation frequency and filter characteristics helped to mitigate the problem. The blue boxes represent the movement detection onset/termination.

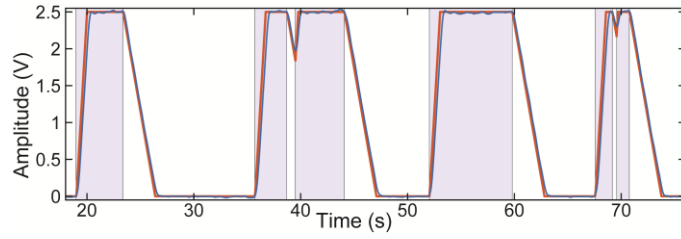


Fig. S10.

Stimulation delivery estimated by two different methodologies. The blue stimulation trace was obtained from filtering the cortical activity with a bandpass filter centered around the stimulation frequency (160Hz). The red stimulation trace was computed from the detection state (internal LDA) and the neurostimulator parameters (amplitude, ramp-up time, ramp-down time, detection onset delay, detection termination delay), leading to a cleaner estimate. The blue boxes represent the movement detection onset/termination.

Table S1. Subject demographics for the study. Total TRS at screening is reported.

Subject ID	Age	Side of Implant	Age at disease onset	TRS Total at screening (before surgical implantation)
ET01	76	Right	57	19
ET02	75	Left	70	23
ET03	78	Left	62	29

Table S2.

DBS and closed-loop settings at each month for each patient during TRS clinical evaluation. If a setting was set as interleaved mode (used only in the OL-case, ET01, month 4) the parameters are separated by a comma. The bandwidth in all cases was 5Hz (centered at the frequency band #1/#2).

Subj ID	month	DBS type	chs	Recording (M1 cortex)				ramp-up (V/s)	ramp-down (V/s)	Retrain		
				freq (Hz)	ampl (V)	pw (μ s)	freq band #1	freq band #2				
ET01	1	OL	1-2+	100	2.4	90	--	--	--	--	--	--
ET01	2	OL	1-2+	130	2.5	120	--	--	--	--	--	--
ET01	3	OL	1-2+	130	2.5	120	--	--	--	--	--	--
ET01	4	OL	1-2+, C+1-	125, 125, 2.2, 2.2	120, 90	--	--	--	--	--	--	--
ET01	4	CL	1-2+	130	0.0-2.5	120	1.00	2.50	12.5 (Hz)	22.5 (Hz)	no	no
ET01	5	OL	0-1+	110	1.8	60	--	--	--	--	--	--
ET01	5	CL	0-1+	110	0.2-1.8	60	0.80	1.60	12.5 (Hz)	22.5 (Hz)	no	no
ET01	6	OL	0-1+	110	0.2-1.8	60	--	--	--	--	--	--
ET01	6	CL	1-2+	180	2.5	60	1.60	0.80	7.5 (Hz)	15 (Hz)	yes	yes
ET02	1	OL	C+2-	180	2.5	90	--	--	--	--	--	--
ET02	2	OL	0-1+	110	0.2-1.8	60	--	--	--	--	--	--
ET02	4	OL	C+1-	180	1.9	60	--	--	--	--	--	--
ET02	5	OL	1-0+	110	2.5	60	--	--	--	--	--	--
ET02	5	CL	1-0+	110	0.0-2.5	60	1.67	4.17	17.5 (Hz)	20 (Hz)	no	no
ET02	6	OL	1-0+	130	2.5	60	--	--	--	--	--	--
ET02	6	CL	1-0+	110	0.0-2.5	60	3.13	4.17	17.5 (Hz)	20 (Hz)	no	no
ET03	1	OL	C+1-	135	2.3	90	--	--	--	--	--	--
ET03	2	OL	C+1-	150	2.0	90	--	--	--	--	--	--
ET03	3	OL	1-2+	160	3.0	90	--	--	--	--	--	--
ET03	3	CL	1-2+	160	0.0-2.5	90	1.67	1.25	15 (Hz)	--	no	no
ET03	4	OL	0-1+	160	3.0	90	--	--	--	--	--	--
ET03	4	CL	0-1+	160	0.0-3.0	90	2.00	1.00	15 (Hz)	--	no	no
ET03	5	OL	0-1+	160	3.0	90	--	--	--	--	--	--
ET03	5	CL	0-1+	160	0.0-2.5	90	2.50	0.83	15 (Hz)	--	no	no
ET03	6	OL	0-1+	160	3.0	90	--	--	--	--	--	--
ET03	6	CL	0-1+	160	0.0-3.0	60	1.50	1.00	15 (Hz)	--	no	no

Table S3.

DBS-related side effects and preference reported. The closed-loop side effects were reported when closed-loop was not yet optimized for minimal side effects. Tolerability to any stimulation induced effects was used as a go/no go milestone at each month.

Subject ID	Continuous DBS side effects (OL-DBS)	Closed-loop DBS side effects (unoptimized)	Closed-loop DBS side effects (optimized, CL-DBS)	Closed-loop DBS side effects during sleep (optimized, CL-DBS)	Preference at 6 months
ET01	None reported	Tingling in left arm	None reported	None reported	None CL-DBS
ET02	Speech impairment, slurring	Tingling in right arm	Minor slurring	None reported	
ET03	None reported	Tingling in right fingers, arm	None reported	None reported	CL-DBS

Movie S1.

Comparison between DBS OFF, closed-loop DBS (fully embedded implementation), and open-loop DBS in ET01 during a volitional movement task. The implant was placed in the right VIM and the left arm was the most affected by tremor pre-DBS. The first part of the video (DBS OFF) shows the patient performing a volitional cup pouring task while revealing visible tremor. The second part of the video (CL-DBS) shows the patient performing a volitional cup pouring and reaching tasks while the tremor is being suppressed on-demand. M1 brain activity (raw channel) was recorded from the implanted Aactiva PC+S in Nexus E mode, together with two power bands centered at 15Hz and 25 Hz using a 5Hz bandwidth. Positive movement detection is shown with blue blocks. The power band information was used by the embedded event detector classifier to control the stimulation output (last row, magenta trace). EMG traces are aligned with the LFP data, and are not used for movement detection. All the data were aligned offline, as the recording was run in Nexus E (embedded) mode. The parameters of the closed-loop were: contacts=1-2+, stim amplitude range=0-2V, ramp-up/down=2V/s, frequency=130Hz, pulse width 120 μ s, classifier update rate: 200ms. The third part of the video (DBS open-loop) shows the patient performing a volitional cup pouring task while tremor is being suppressed. The parameters for the open-loop were: contacts=1-2+, stim amplitude=2.5V, frequency=130Hz, pulse width 120 μ s.

Movie S2.

Comparison between DBS OFF, closed-loop DBS (fully embedded implementation), and open-loop DBS in ET02 during a cued-go cup reaching task. The implant was placed in the left VIM and the right arm was most affected by tremor pre-DBS. The first part of the video (DBS OFF) shows the patient performing the reaching task while revealing visible tremor. The second part of the video (CL-DBS) shows the patient performing the reaching task while tremor is being suppressed on-demand. M1 brain activity (raw channel) was recorded from the implanted Aactiva PC+S in Nexus E mode, together with two power bands centered at 20Hz and 17.5Hz using a 5Hz bandwidth. Positive movement detection is shown with blue blocks. The power band information was used by the embedded event detector classifier to control the stimulation output (last row, magenta trace). EMG traces, not used for movement detection, are aligned with the LFP data, with movement execution labeled in violet. Yellow blocks indicate when the subject was asked to prepare to move the cued arm. All the data were aligned offline, as the recording was run in Nexus E (embedded) mode. The parameters of the closed-loop were: contacts=1-0+, stim amplitude range=0-2V, ramp-up/down=1.67/0.57 V/s, frequency=110Hz, pulse width 60 μ s, classifier update rate: 200ms. The third part of the video (DBS open-loop) shows the patient performing the reaching task while tremor is being suppressed. The parameters for the open-loop were: contacts=1-0+, stim amplitude=2.5V, frequency=130Hz, pulse width 60 μ s.

Movie S3.

Comparison between DBS OFF, closed-loop DBS (fully embedded implementation), and open-loop DBS in ET03 during a volitional cup reaching task. The implant was placed in the left VIM and the right arm was the most affected by tremor pre-DBS. The first part of the video (DBS OFF) shows the patient performing a volitional cup pouring task while revealing visible tremor. The second part of the video (CL-DBS) shows the patient performing the volitional cup

pouring task while tremor is being suppressed on-demand. M1 brain activity (raw channel) was recorded from the implanted Aactiva PC+S in Nexus E mode, together with two power bands centered at 15Hz using a 5Hz bandwidth. Positive movement detection is shown with blue blocks. The power band information was used by the embedded event detector classifier to control the stimulation output (last row, magenta trace). EMG traces are aligned with the LFP data, and are not used for movement detection. All the data were aligned offline, as the recording was run in Nexus E (embedded) mode. The parameters of the closed-loop were: contacts=0-1+, stim amplitude range=0-3.0V, ramp-up/down=2/1.5 V/s, frequency=160Hz, pulse width 90 μ s, classifier update rate: 200ms. The third part of the video (DBS open-loop) shows the patient performing a volitional cup pouring task while tremor is being suppressed. The parameters for the open-loop were: contacts=0-1+, stim amplitude=3.0V, frequency=160Hz, pulse width 90 μ s.